Late-Twentieth-Century Simulation of Arctic Sea Ice and Ocean Properties in the CCSM4

ALEXANDRA JAHN,* KARA STERLING,+ MARIKA M. HOLLAND,* JENNIFER E. KAY,* JAMES A. MASLANIK,# CECILIA M. BITZ,@ DAVID A. BAILEY,* JULIENNE STROEVE,& ELIZABETH C. HUNKE,** WILLIAM H. LIPSCOMB,** AND DANIEL A. POLLAK++

* *National Center for Atmospheric Research,## Boulder, Colorado*
+ *International Arctic Research Center, University of Alaska at Fairbanks, Fairbanks, and NOAA/NWS/West Coast and Alaska Tsunami Warning Center, Palmer, Alaska*
# *Colorado Center for Astrodynamics Research, University of Colorado, Boulder, Colorado*
@ *Department of Atmospheric Sciences, University of Washington, Seattle, Washington*
& *National Snow and Ice Data Center, Cooperative Institute for Research in Environmental Sciences, University of Colorado, Boulder, Colorado*
** *Climate, Ocean and Sea Ice Modeling Program, Los Alamos National Laboratory, Los Alamos, New Mexico*
++ *College of Earth and Mineral Sciences, The Pennsylvania State University, University Park, Pennsylvania*

(Manuscript received 14 April 2011, in final form 31 August 2011)

ABSTRACT

To establish how well the new Community Climate System Model, version 4 (CCSM4) simulates the properties of the Arctic sea ice and ocean, results from six CCSM4 twentieth-century ensemble simulations are compared here with the available data. It is found that the CCSM4 simulations capture most of the important climatological features of the Arctic sea ice and ocean state well, among them the sea ice thickness distribution, fraction of multiyear sea ice, and sea ice edge. The strongest bias exists in the simulated spring-to-fall sea ice motion field, the location of the Beaufort Gyre, and the temperature of the deep Arctic Ocean (below 250 m), which are caused by deficiencies in the simulation of the Arctic sea level pressure field and the lack of deep-water formation on the Arctic shelves. The observed decrease in the sea ice extent and the multiyear ice cover is well captured by the CCSM4. It is important to note, however, that the temporal evolution of the simulated Arctic sea ice cover over the satellite era is strongly influenced by internal variability. For example, while one ensemble member shows an even larger decrease in the sea ice extent over 1981–2005 than that observed, two ensemble members show no statistically significant trend over the same period. It is therefore important to compare the observed sea ice extent trend not just with the ensemble mean or a multimodel ensemble mean, but also with individual ensemble members, because of the strong imprint of internal variability on these relatively short trends.

1. Introduction

The Arctic Ocean has undergone substantial changes in recent decades, including warm anomalies of the Atlantic layer in the Arctic Ocean (e.g., Quadfasel et al. 1991; Polyakov et al. 2005), changes in the liquid freshwater (FW) storage in the Beaufort Gyre (Proshutinsky et al. 2009; McPhee et al. 2009), and the well-known decrease in the summer sea ice extent (e.g., Stroeve et al. 2008), which has set several successive record minima during the last decade and has exceeded all but a few of the Coupled Model Intercomparison Project phase 3 (CMIP3) model predictions over the satellite era (Stroeve et al. 2007). Concurrent to the decline in the sea ice extent, the sea ice thickness in the Arctic has also decreased (e.g., Rothrock et al. 1999; Tucker et al. 2001; Haas et al. 2008; Giles et al. 2008; Kwok et al. 2009). Climate simulations for the twenty-first century predict additional large changes in the Arctic and subarctic regions, among them an intensification of the hydrological cycle in the Arctic

The National Center for Atmospheric Research is sponsored by the National Science Foundation.

Corresponding author address: Alexandra Jahn, P.O. Box 3000, National Center for Atmospheric Research, Boulder, CO 80307-3000.
E-mail: ajahn@ucar.edu

DOI: 10.1175/JCLI-D-11-00201.1

(Arnell 2005), an increase in the liquid FW export from the Arctic Ocean (Holland et al. 2007; Vavrus et al. 2012), and summer ice-free conditions either by or before the end of the twenty-first century (e.g., Zhang and Walsh 2006; Holland et al. 2006b). Because of the many potential consequences of the sea ice decline on the environment (e.g., see the Arctic Climate Impact Assessment 2005), the survival of animal species in the Arctic (e.g., Durner et al. 2009), and economic activities (see the Arctic Climate Impact Assessment 2005), the interest in sophisticated predictions of future Arctic climate change has increased in light of the rapid changes in the summer sea ice extent over the past decade. Holland et al. (2010) showed that models with a thicker and more extensive Arctic sea ice cover showed smaller decreases in the summer sea ice extent over the late-twentieth and twenty-first century than models with more realistic late-twentieth-century sea ice distributions. Hence, a detailed knowledge of the biases of the simulated twentieth-century Arctic climate is important in order to evaluate the skill of climate model projections for the Arctic in the twenty-first century.

The previous version of the Community Climate System Model (CCSM), the CCSM, version 3 (CCSM3), has been widely used for studies of Arctic processes and Arctic climate change and has been shown to perform quite well (e.g., Bitz et al. 2006; Holland et al. 2006c,b,a, 2007, 2010; Vavrus and Waliser 2008; Deser et al. 2010; Jahn et al. 2010; Vavrus et al. 2011). A comprehensive validation of Arctic sea ice and ocean properties in simulations of the CCSM3 (or from any global climate model, for that matter), however, has never been done. The purpose of the present article is to fill this gap for the newest version of the CCSM, the CCSM, version 4 (CCSM4), by comparing its late-twentieth-century simulation of the Arctic sea ice and ocean state with available data for this period. Most of the data products used for this comparison have only recently become available, making a detailed Arctic-wide validation of the simulated sea ice and ocean properties possible for the first time.

The analysis shows that the model captures the mean state of the sea ice and ocean in the Arctic as well as changes in the sea ice cover during recent decades reasonably well. Shortcomings in the model are mainly found in the sea ice motion field, the location and strength of the Beaufort Gyre, and the deep Arctic Ocean temperatures. A similar analysis focused on the Arctic atmospheric CCSM4 simulations is shown in de Boer et al. (2012). The knowledge about CCSM4's performance for several key variables of the Arctic climate will allow a critical evaluation of twenty-first-century simulations, as, for example, described in Vavrus et al. (2012), and should also be a useful reference for other Arctic climate studies with the CCSM4.

2. Model

a. CCSM4

The CCSM4 is a fully coupled global climate model that conserves mass and energy and does not use flux adjustments (Gent et al. 2011). It consists of modules for the atmosphere, ocean, sea ice, and land, which are coupled at regular intervals through a coupler. All components have been updated compared to CCSM3, and some of the changes most relevant to the Arctic are described below. More details on the improvements can be found in the individual model descriptions referenced below.

The atmospheric model is the Community Atmospheric Model, version 4 (CAM4), which has a horizontal resolution of $1.25° \times 0.9°$ and 26 layers in the vertical [see R. B. Neale et al. (2011, personal communication) for a detailed documentation of CAM4]. Among the many important improvements in CAM4, the most important for the Arctic climate is the addition of a freeze-dry modification, which reduces the amount of wintertime low clouds in the Arctic (Vavrus and Waliser 2008). The land model of the CCSM4 is the Community Land Model, version 4 (CLM4), which has the same horizontal resolution as the atmospheric model. It has been updated with many new datasets and many new capabilities, among them the addition of solid runoff, which improves global energy conservation [see Lawrence et al. (2011) for a full documentation of the CLM4].

The ocean model of the CCSM4 is based on the Parallel Ocean Program, version 2 (POP2), with a 1° rotated orthogonal grid, a North Pole that is displaced to Greenland, and 60 vertical levels, ranging from a thickness of 10 m at the surface to 200–250 m at depth [see Smith et al. (2010) for a full documentation]. Among the many improvements are the addition of a near-surface eddy flux parameterization, a submesoscale mixing scheme, an abyssal tidally driven mixing parameterization, a deep overflow parameterization, and vertically varying thickness and isopycnal diffusivity coefficients. Details of the ocean model simulations are described in Danabasoglu et al. (2012).

The sea ice model of the CCSM4 is the Los Alamos Sea Ice Model (CICE) version 4, also known as the Community Ice Code (Hunke and Lipscomb 2008). It is a dynamic–thermodynamic model that includes a subgrid-scale ice thickness distribution (Thorndike et al. 1975; Lipscomb 2001), energy-conserving thermodynamics (Maykut and Untersteiner 1971; Bitz and Lipscomb 1999), and elastic–viscous–plastic (EVP) dynamics (Hunke and Dukowicz 1997). Important changes compared to earlier versions include an improved ridging scheme (Lipscomb et al. 2007) and a new shortwave

radiation scheme (Briegleb and Light 2007). The latter allows for the incorporation of melt ponds and absorbers, like dust and black carbon, which overall lead to a more sophisticated and internally consistent treatment of surface albedo and result in much more realistic surface ice albedos than those used in the CCSM3. These new parameterizations in the shortwave radiation scheme and their effect on the simulation of the Arctic sea ice cover are described in detail in Holland et al. (2012).

b. Simulations

The analysis presented in this article is mainly based on six ensemble members from the twentieth-century simulations with the CCSM4 (Gent et al. 2011), which span the period of 1850–2005 following the Intergovernmental Panel on Climate Change (IPCC) CMIP, version 5 (CMIP5) protocol. Results from the long 1850 control simulation with the CCSM4 are also discussed in some places. The main focus of this article are the present-day climatological mean features of the Arctic Ocean and its sea ice cover as well as trends in the sea ice over recent decades. In agreement with other papers in the special issue of the *Journal of Climate* devoted to CCSM4 (e.g., de Boer et al. 2012), and to allow a comparison with satellite data, 1981–2005 is taken as being representative for the present-day climate unless data are only available for shorter periods. The data used for the comparison with the model are described in each subsection, to make it possible to discuss the differences between the data and the model simulation together with the results.

3. Arctic sea ice

Several important characteristics of the simulated Arctic sea ice cover can now be constrained by satellite-derived sea ice products that not only resolve the climatological mean, but can often also give us information on the variability of the sea ice cover since the early 1980s. In the following five subsections (sections 3a–3e) we use several satellite-derived products to assess how well the CCSM4 simulates the late-twentieth-century Arctic sea ice concentration, sea ice extent, sea ice thickness, multiyear sea ice cover, sea ice motion, and the timing of melt onset and freeze up.

a. Sea ice concentration and extent

To assess how well the CCSM4 simulates the sea ice concentration, we use the sea ice concentration from Comiso (1999), which is derived using the Advanced Microwave Scanning Radiometer for Earth Observing System (EOS) (AMSR-E) bootstrap algorithm applied to the brightness temperature data from the Scanning Multichannel Microwave Radiometer (SMMR) on the *Nimbus-7* satellite and from three Special Sensor Microwave Imager (SSM/I) sensors on the Defense Meteorological Satellite Program's (DMSP's) *F8*, *F11*, and *F13* satellites. We find that the simulated spatial sea ice concentration pattern as well as the location of the sea ice edge (defined as 15% ice concentration contour) is in close agreement with the SSMR and SSM/I satellite data (Comiso 1999; see Fig. 1). The main differences occur in September and include a high bias in ice concentration in Baffin Bay, a low bias in ice concentration in the coastal waters of the Beaufort Sea, and an overall low bias in central Arctic ice concentration. In March, the most notable bias is a too-extensive sea ice cover in parts of the North Pacific and in the Nordic Sea close to Iceland. Compared to the CCSM3, however, the sea ice concentration is much improved, as shown in Fig. 6 in Gent et al. (2011).

To evaluate the simulated temporal variability of the sea ice cover, we use the sea ice extent index, calculated for areas with at least 15% sea ice concentration. To assess the uncertainty in the satellite-derived sea ice extent resulting from the use of different algorithms, we use two satellite-derived sea ice extents in the following, which are based on data from the same satellites: one of them is the National Snow and Ice Data Center (NSIDC) sea ice extent index from Fetterer et al. (2002), which is calculated from the sea ice concentrations generated using the National Aeronautics and Space Administration (NASA) Team algorithm (Cavalieri et al. 1999); and the other one is calculated from the sea ice concentration data of Comiso (1999), which we will refer to as the bootstrap sea ice extent in the following because it is derived using the AMSR-E bootstrap algorithm.

For 1981–2005, the average ensemble mean September sea ice extent of 7.28 million km^2 is in good agreement with the NSIDC and bootstrap sea ice extents for the same period (6.81 million and 7.22 million km^2, respectively). The CCSM4 also captures the magnitude and timing of the seasonal cycle of the sea ice extent very well, as shown in Fig. 2a. Again, the largest differences occur in summer, but this bias is small compared to the spread between the NSIDC sea ice extent (solid line) and the bootstrap sea ice extent (dashed line). Furthermore, in summer, the sea ice concentration from passive microwave data from satellites tends to be underestimated, due to the presence of melt ponds (Steffen et al. 1992). Compared to the CCSM3 (see Fig. 2 in Holland et al. 2006c), the seasonal cycle of the sea ice extent from the CCSM4 agrees much better with the satellite data, especially in winter, where the CCSM3 overestimated the sea ice extent because of excessive sea ice in the Labrador Sea.

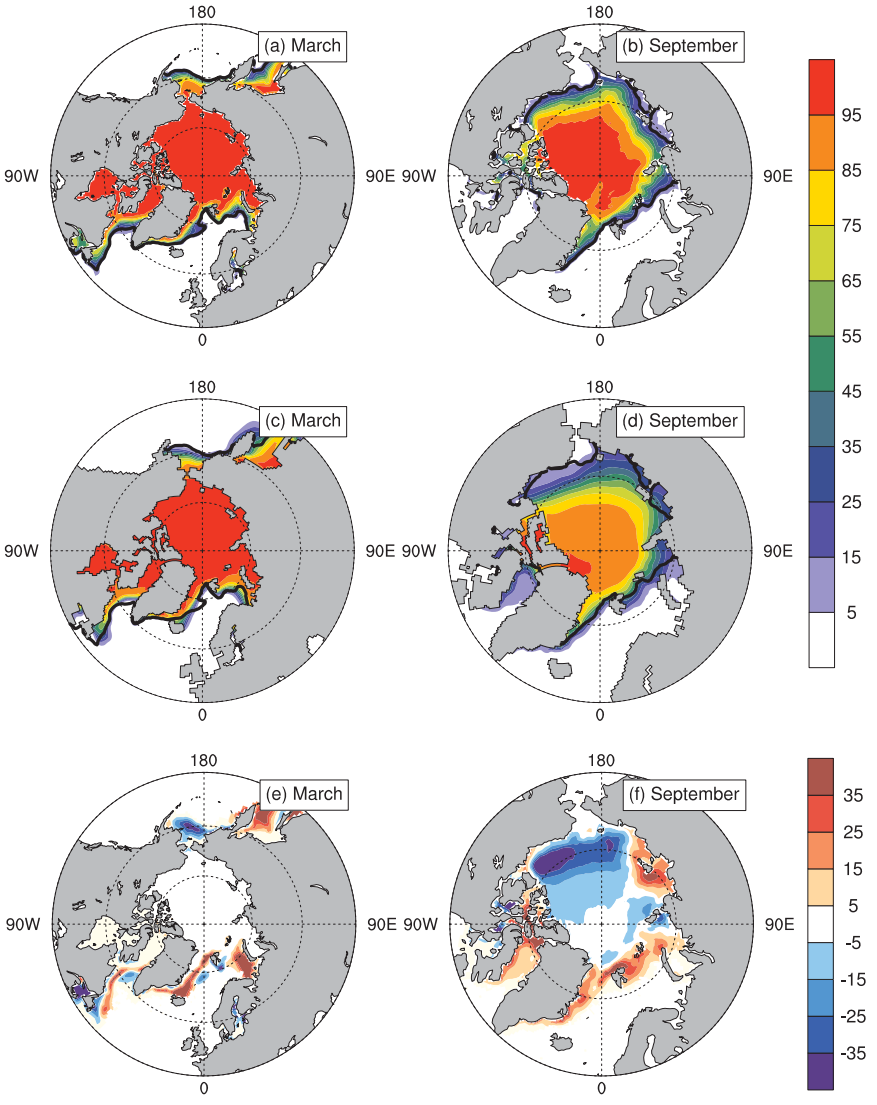

FIG. 1. SSM/I and SSMR (Comiso 1999) climatological sea ice concentration (%) compared to the six member CCSM4 ensemble average sea ice concentration for 1981–2005 for (a),(c) March and (b),(d) September. The ice edge (taken as 15% sea ice concentration contour) from the SSM/I and SSMR data are shown as black line. (e),(f) The difference between the CCSM4 and the SSM/I and SSMR ice concentration, showing regions with too much ice in the simulation (red colors) and regions with not enough ice in the simulation (blue).

The interannual variability of the September sea ice extent in the individual ensemble members shows a similar magnitude as that seen in the satellite data (see Fig. 2b), and a downward trend is clearly visible in both observations (red lines), the individual ensemble members (thin blue lines), and the ensemble mean (thick blue line). The least squares regression trend in the September sea ice extent for 1981–2005 is the same for both satellite products and is bracketed by the trends in the six ensemble members (see Table 1, and the green cross versus the green circles in Fig. 3). The trend in the ensemble mean is slightly larger than ½ of the satellite-derived trends (see Table 1). As the ensemble mean is a better representation of the forced trend, because the internal variability (the variability intrinsic to a climate state) in the individual ensemble members is partially averaged out, this suggests a large influence of internal variability on the satellite-derived sea ice extent trends. All of these trends except for the two least negative individual CCSM4 trends are significantly different from the null hypothesis of no trend, with a confidence level of over 95% according to a two-sided Student's

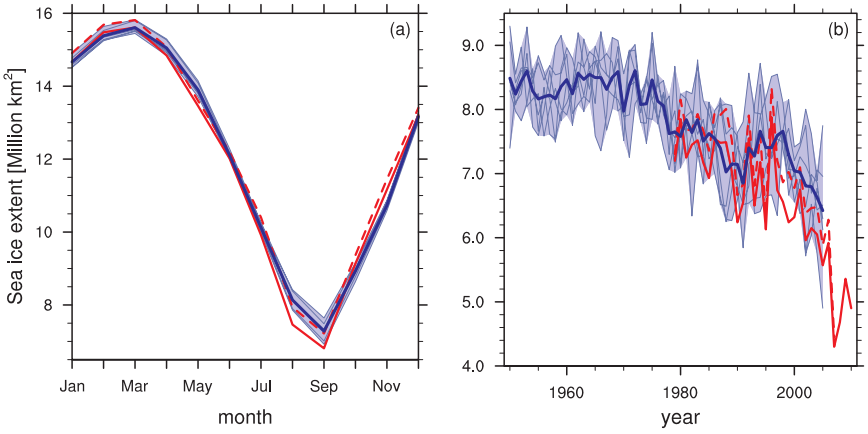

FIG. 2. (a) Climatological seasonal cycle (1981–2005) and (b) time series of the sea ice extent from satellite data (red lines) and the CCSM4 (blue lines). The CCSM4 ensemble mean (blue) and the spread between the ensemble members (shaded area) are shown, with individual ensemble members (thin blue lines) also indicated. To show the spread in the satellite data resulting from the use of different retrieval algorithms, the NSIDC sea ice extent (Fetterer et al. 2002; solid red line) and the bootstrap sea ice extent calculated from the sea ice concentrations from Comiso (1999; dashed red line) are plotted. The sea ice extent is calculated as the area with a sea ice concentration of 15% or more, and in the satellite data gap around the North Pole the area is assumed to be covered by at least 15% at all times.

t test (see Table 1). In other words, approximately one in three ensemble members has a sea ice extent trend for 1981–2005 that is not statistically significant, which again highlights that the internal variability is large and can hide (or amplify) a forced trend over this relatively short period, complicating the detection of a forced trend. Over longer periods (1970–2005, or longer), however, all ensemble members show a decreasing trend in the ice extent that is significant at the 95% level, resulting from the smaller contribution of internal variability compared to the trend.

A closer analysis of the sea ice changes in the individual ensemble members reveals that in one of the two ensemble members where the sea ice extent does not show a significant negative trend over 1981–2005, the ice in the Arctic stays relatively old up until 2005, resulting from the specific variability of the atmospheric forcing in this run. This older and thicker Arctic ice cover leads to a smaller decrease of the September ice extent because the area covered by less than 15% sea ice does not decrease strongly. However, the ice is still melting over the 1981–2005 period, as evidenced by the significant trend in the ice area and ice volume time series (not shown). In the other ensemble member without a significant negative sea ice extent trend for 1981–2005, the ice extent already decreases very strongly in the late 1970s, with only a small decrease since then, again resulting from the specific atmospheric variability in that simulation. However, all ensemble members show a significant negative trend in the sea ice area over 1981–2005. This stronger influence of internal variability on the sea ice extent compared to the sea ice area is present because the ice extent trend does not take into account the decreasing concentration of the ice cover in the Arctic as long as it stays above 15% (because all areas with an ice concentration of 15% or more are counted as ice covered when computing the sea ice extent), whereas the ice area is the area actually covered by ice. Despite this problem with the sea ice extent definition we chose to compare the sea ice extents rather than the sea ice areas, because the satellite-derived sea ice measurements have a data gap around the North Pole that is commonly filled with 100% ice cover, making a comparison of satellite-derived and modeled sea ice areas questionable.

TABLE 1. Least squares regression trends (%) in the sea ice extent for 1981–2005 (% decade^{-1}), calculated from the satellite-derived NSIDC and bootstrap sea ice extents and the six CCSM4 ensemble simulations. The CCSM4 ensemble-mean sea ice extent trend is shown (in bold) in the last column of the table. Trends that are not significantly different from the null hypothesis of no trend with a confidence level of over 95% are shown in parentheses.

	NSIDC	Bootstrap	CCSM4						
Trends	−9.0	−9.0	−11.0	−7.2	−6.0	−4.4	(−1.0)	(−0.5)	**−5.0**

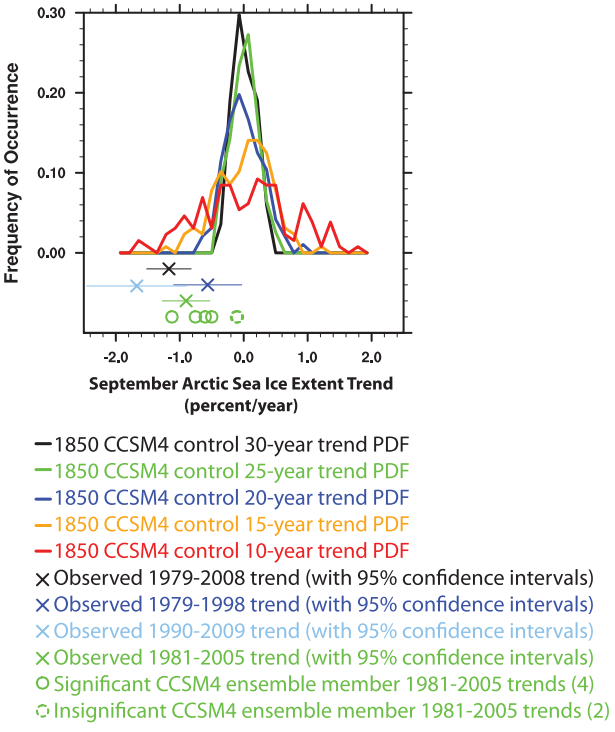

FIG. 3. Probability density function (PDF) of September sea ice extent trends (percent change per year) for different periods from the 1300-yr-long 1850 control simulation with the CCSM4 (b40.1850.track1.1deg.006). To evaluate whether trends computed over different lengths of time are likely to be outside the internal variability, as represented by trends in the 1300-yr-long CCSM4 1850 control simulation, trends calculated from the satellite-derived NSIDC sea ice extent (crosses; Fetterer et al. 2002) for different periods and the trends from the six individual ensemble members of the twenty-first-century simulation for 1981–2005 (circles) are shown. The trends that are not statistically significant at the 95% level are shown as dashed circles (note that the two not significant trends from the model are almost the same and are plotted on top of each other) and the 95% confidence intervals of the observed trends are shown as thin horizontal lines through the crosses.

The important role of internal variability and its effect on trend detection in climate simulations was also discussed in Deser et al. (2011), and it was shown that, depending on the climatic variable (i.e., temperature, sea level pressure, precipitation, etc.), different numbers of ensemble members are needed to detect a forced trend in the ensemble mean. Using the same approach as that used in Deser et al. (2011), we find that for the Arctic sea ice extent trend over 1981–2005, we need at least five ensemble members to identify the forced trend in the ensemble mean at the 95% significance level if we make no assumption about the sign of the trend. The six-member ensemble we have used here is therefore just large enough to detect a forced trend in the ensemble mean for the short 1981–2005 period, but, as seen earlier, the forced trend cannot be detected in each individual ensemble member because of the large imprint of internal variability. For the longer 1950–2005 period, on the other hand, only one ensemble members is needed to detect a forced trend in the sea ice extent over 1950–2005, in agreement with the earlier results that all ensemble members have a significant negative sea ice extent trend over 1950–2005.

The influence of internal variability on relatively short trends is also clearly shown by the probability density functions of ice extent trends of different lengths in the 1300-yr-long 1850 control simulation with the CCSM4 (see Fig. 3). Unsurprisingly, trends calculated over shorter periods show a wider distribution of possible trends resulting from internal variability than trends calculated over longer periods. Perhaps more surprisingly, we find that three of the 25-yr model trends for 1981–2005 (the three right-most green circles in Fig. 3) are not outside the range of 25-yr trends because of internal variability in the 1850 control simulation with the CCSM4 (green line in Fig. 3), despite the fact that one of these trends is statistically significant at the 95% level. The remaining two 1981–2005 model trends (the two left-most green circles in Fig. 3), as well as the observed 25- and 30-yr trends between 1979 and 2008 (see the black and green crosses in Fig. 3), are outside the range of internal variability. For the observed 20-yr trends, it depends on the period over which the trend is calculated: the observed 1979–98 trend (dark blue cross in Fig. 3) is not outside the range of internal variability simulated by the CCSM4, whereas the more recent 20-yr trend over 1990–2009 (light blue cross in Fig. 3) is well outside the range of internal variability from the CCSM4. Note, however, that the probability density function of the internal variability based on the CCSM4 1850 control simulation is probably biased narrow compared to the internal variability in the late-twentieth century, because previous studies have shown that the standard deviation of the sea ice extent increases as the sea ice thins (Holland et al. 2008). Nevertheless, this analysis highlights that while trends calculated over 20 or 25 yr might be statistically significant at the 95% level, it is important to keep in mind that internal variability might still have a relatively large imprint on the magnitude of these trend [for more details about sea ice extent trends in the CCSM4 over different periods in a warming world, see Kay et al. (2011)].

b. *Sea ice thickness*

Large-scale gridded sea ice thickness data for the Arctic have only recently started to become available and are based on satellite altimeter measurements (e.g., Laxon et al. 2003; Kwok et al. 2004). Here we use the gridded sea ice data from Kwok et al. (2009), which are derived from Ice, Cloud, and Land Elevation Satellite

(ICESat) measurements [see Kwok and Cunningham (2008) for details on the method] and are thus far limited to 1-2–month periods in the spring and fall of 5 yr (2003/04–2007/08). As shown in Figs. 4a–d, the large-scale pattern of the sea ice thickness for the ensemble mean 5-yr average over 2001–05 shows the same main characteristics that are also seen in the ICESat-derived sea ice thickness, given the differences in the resolution of the data (25 km × 25 km in the ICESat-derived ice thickness and 1° in the CCSM4 simulation, which, averaged over the Arctic, translates to a resolution of about 65 km × 30 km). The largest bias in the model appears to be a too-small area of very thick ice (>4 m) north of Greenland and the Canadian Arctic Archipelago (CAA) in both spring and fall, as well as too-thick ice in the Eurasian shelf seas (by about 1 m), mainly in winter. Because of the strong influence of atmospheric forcing on the sea ice thickness patterns and the short 5-yr record, a perfect match between the 5-yr averages from the satellite data and the CCSM4 simulations is not expected. The strong impact of interannual variability on ice thickness in the observational record leads to a better match between 5-yr averages from individual ensemble members and the ICESat data than with the six-member ensemble mean (compare Figs. 4e,f to Figs. 4a,b and Figs. 4c,d). Furthermore, individual years from ensemble members show an even closer match to individual years of the observed sea ice thickness pattern than the 5-yr averages (not shown).

Another way to compare ICESat-retrieved ice thickness data and the simulated sea ice thickness is to look at the histogram of the fraction of the ice-covered area that is occupied by ice of a certain thickness (see Fig. 5). This sea ice thickness histogram (for the area covered by the satellite data) confirms that the ensemble mean gridcell-averaged ice thickness from the CCSM4 is in good agreement with the ICESat retrievals of the average ice thickness. In agreement with the spatial plots in Fig. 4, the histogram for both spring and fall shows that the most common gridcell mean sea ice in the CCSM4 simulation is 0.5 m thicker than that in the ICESat retrieval, but at the same time the CCSM4 does not simulate enough very thick (>3.5 m) sea ice. In addition, the histogram also reveals that the CCSM4 has too much very thin ice (<0.5 m) in fall. Given the changes in the simulated sea ice thickness distribution between 1981–85 and 2001–05 (see the dashed versus the solid black lines in Fig. 5), part of these differences could be due to the fact that we are comparing 5-yr averages over slightly different periods of a strongly variable field that is undergoing a rapid transition. Furthermore, it is likely that the differences in the spatial resolution (by a factor of 2 or 3) between the two datasets also affect the gridcell-averaged sea ice thickness distribution. Finally, most of the differences between the thickness distributions are within the error bars on the ICESat ice thickness retrievals [approximately 0.7 m, see Kwok and Cunningham (2008)]. We therefore conclude that the model is able to simulate the large-scale pattern of the gridcell-averaged Arctic sea ice thickness reasonably well. Compared to the CCSM3 (see Fig. 1 in Holland et al. 2006c), the sea ice thickness simulation is improved in the CCSM4, and the erroneous secondary sea ice maximum in the Chukchi and East Siberian Sea is no longer present in the CCSM4 simulations.

c. *Multiyear sea ice cover*

Because older ice tends to be thicker, it is less likely to melt out during summer than first-year ice. Simulating a realistic amount and spatial distribution of multiyear ice is therefore important in order to resolve sea ice cover trends. To evaluate the multiyear ice cover simulated by the CCSM4, we make use of the sea ice ''age'' dataset of Fowler et al. (2003) and described further by Maslanik et al. (2007, 2011), Tschudi et al. (2010) and Stroeve et al. (2011). To summarize the Fowler et al. (2003) approach briefly, ice movement is calculated using a cross-correlation technique applied to sequential, daily satellite images acquired by the SMMR and SSM/I passive microwave brightness temperature sensors, and visible and thermal observations from the Advanced Very High Resolution Radiometer (AVHRR) sensors. Motion vectors are then blended via optimal interpolation with International Arctic Buoy Program (IABP) drifting-buoy vectors. Ice age is estimated by treating each grid cell that contains ice as a discrete, independent Lagrangian particle and transporting the particles at weekly time steps. The process is similar to that used by Rigor and Wallace (2004) for the IABP buoys, but adapted to use the finer-resolution, more spatially distributed satellite-derived motion fields. Gridded maps of the ice age data, projected to the NSIDC Equal-Area Scalable Earth (EASE) grid at 12.5 km × 12.5 km cell size, are then created by assigning to each grid cell the age of the oldest particle that lies within the cell domain. Particles are treated as ''open water'' if the ice concentration at the particle's grid cell is less than 15%, as defined using the NASA Team algorithm applied to SSM/I and SSMR brightness temperatures. Grid cells of multiyear ice therefore represent the extent of the multiyear ice cover, which means that it is covered with at least 15% multiyear ice (as opposed to representing areas with substantial multiyear ice coverage). It is also important to note that even in locations indicated as open water in the age fields, some ice, and even some multiyear ice, may be present, particularly during

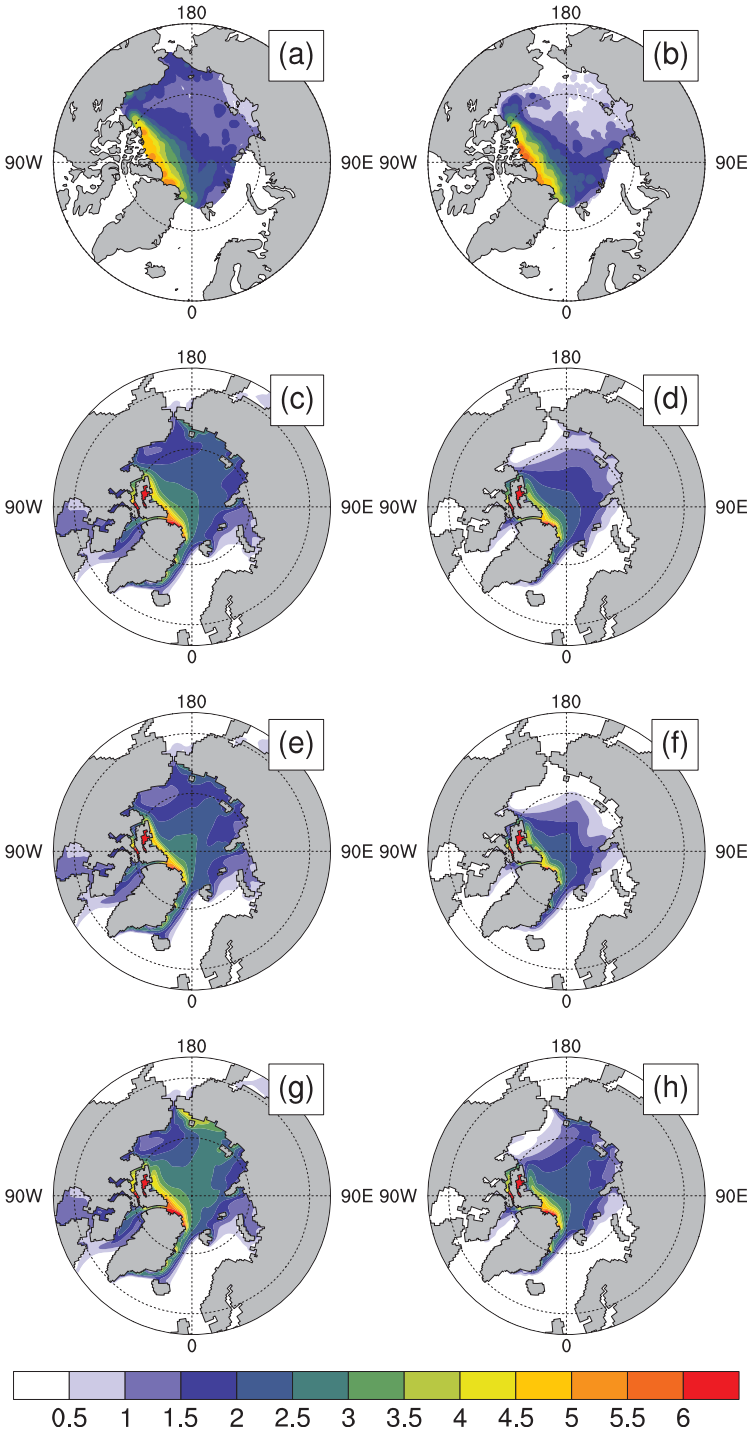

FIG. 4. Sea ice thickness (m) from (a),(b) ICESat data (Kwok et al. 2009) and (c)–(h) CCSM4 for (left) February–March and (right) October–November. The ICESat data are averaged over fall 2003–07 and spring 2004–08. The CCSM4 sea ice thickness is from years 2001–05 of the twentieth-century simulations and is the gridcell mean ice thickness. The ensemble average of all six ensemble members is shown in (c) and (d). To illustrate the large spread between the individual ensemble members for this period, the sea ice thickness pattern for the ensemble member with the overall (e),(f) smallest and (g),(h) largest extent of thick ice in the Arctic during this period is shown. Note that the ICESat data do not show the full Northern Hemisphere sea ice, but are limited to the central Arctic Ocean. The ICESat data are available online (http://rkwok.jpl.nasa.gov/icesat/download.html).

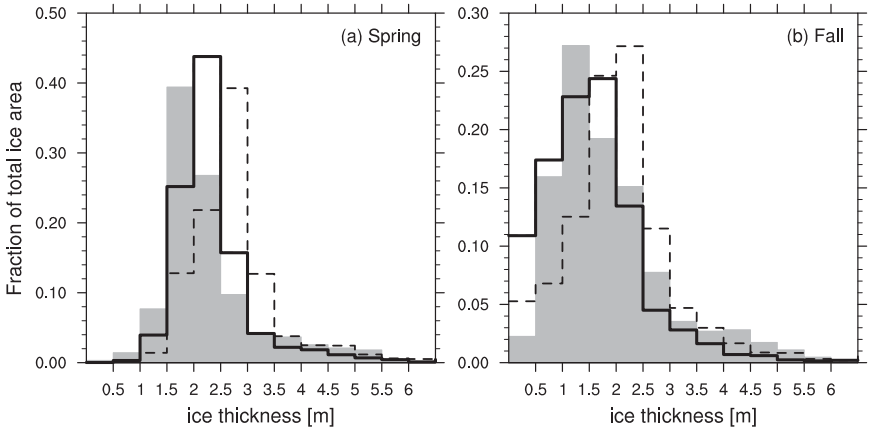

FIG. 5. Histogram of the sea ice thickness (m) distribution in the Arctic Ocean for (a) spring (February–March) and (b) fall (October–November), normalized by the fraction of the total ice area covered by sea ice of a certain thickness. The ICESat data (Kwok et al. 2009; gray shading) are averaged over 2004–07 for the spring data and 2003–08 for the fall data (as in Fig. 4). The CCSM4 ensemble mean gridcell-averaged ice thickness is shown for 2001–05 (solid black line) and 1981–85 (dashed black line). Because the ICESat data do not cover the entire sea ice–covered region in the Northern Hemisphere, especially in spring (see Fig. 4), the Barents Sea, CAA, and Baffin and Hudson Bays have been masked in the model data to mimic the coverage of the ICESat data.

summer melt (Markus and Dokken 2002; Agnew and Howell 2003).

In the model, first-year ice is tracked using Eulerian tracers and is defined as ice that has not yet survived a September ice minimum. The multiyear ice fraction is then computed by subtracting the first-year ice concentration from the total ice concentration. In addition to these differences in how multiyear ice is computed, the resolution of the CCSM4 is significantly lower than the resolution of the satellite-derived ice age data described above (approximately 65 km $\times$ 30 km for the CCSM4 in the Arctic versus 12.5 km $\times$ 12.5 km for the satellite-derived product).

Despite these differences between the satellite-derived and model-simulated multiyear ice cover, the general agreement between the two datasets is remarkably good, as can be seen when looking at the frequency of the multiyear sea ice coverage of a grid cell in a 5-yr period (Figs. 6a–d). This comparison shows that the model correctly captures the areas where multiyear ice is present frequently and also shows the decrease in the multiyear ice cover, especially over the shelf seas, between the beginning of the satellite era and the early twenty-first century. This decrease in multiyear sea ice is also clearly visible if we look at the temporal evolution of the multiyear sea ice extent (see Fig. 7). However, because of the much larger grid boxes, the multiyear sea ice extent from the model is much larger than that shown by the data, as it includes all grid cells with at least 15% multiyear ice cover. Comparing the multiyear ice area would therefore be more accurate, because then grid cells are not assumed to be 100% covered by multiyear ice and the size of grid cells is less important. However, because the satellite-derived data contain the maximum ice age, rather than the fractional coverage of multiyear ice in each grid box, we cannot compute the multiyear ice area from it. Hence, because of all of these differences between the satellite-derived multiyear ice data and the CCSM4 multiyear ice data, it is impossible to directly compare them. Nevertheless, the comparison of both the multiyear sea ice extent and the multiyear sea ice area from the model with the multiyear sea ice extent from Fowler et al. (2003) shows that the CCSM4 simulates an overall reasonable multiyear ice cover (see Fig. 7). Note that the spread between the individual ensemble members is again large, as shown in Figs. 6e–h and by the thin gray lines and the shading in Fig. 7. As mentioned earlier, this different evolution of the age structure of the Arctic sea ice cover leads to differences in the sea ice extent trend and highlights the important role of internal variability superimposed on the overall negative trend in Arctic sea ice.

d. Sea ice motion

To assess the simulated sea ice motion field, we compare it with the polar pathfinder sea ice motion data, which is computed from a combination of satellite products (AVHRR, SMMR, and SSM/I) and the IABP buoy data (Fowler 2003). As shown in Figs. 8a,b, the mean 1981–2005 simulated ice motion in winter

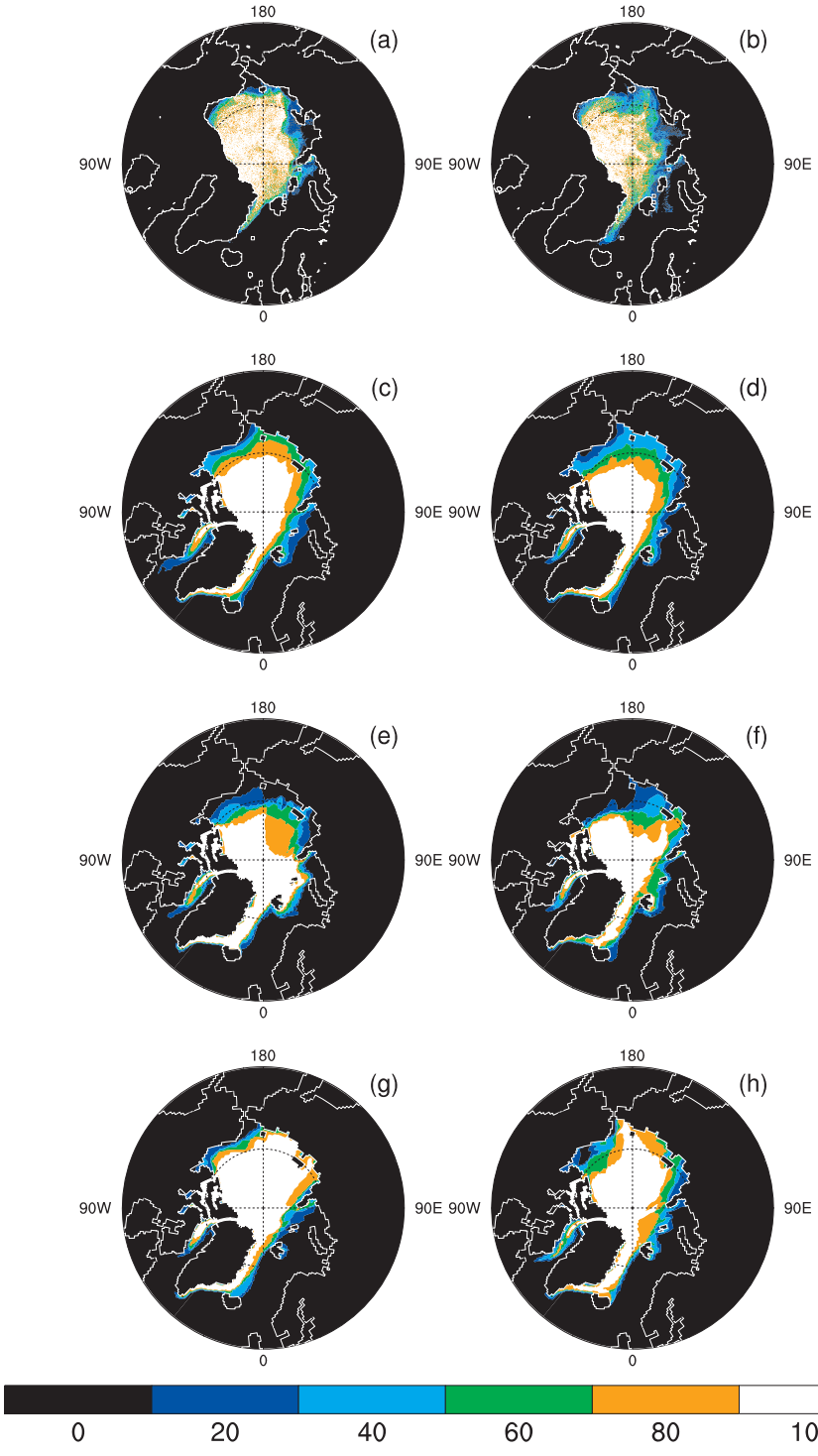

FIG. 6. Frequency of multiyear (>1 yr) sea ice cover during March in (a),(b) the satellite-derived ice age product (see the text for details on the data) and (c),(d) the ensemble mean of the CCSM4 for (left) 1981–85 and (right) 2001–05. To show the spread among the individual ensemble members, the ensemble members with the (e),(f) minimum and (g),(h) maximum multiyear sea ice cover in each period are shown. The frequency is shown as percentage of occurrence of multiyear sea ice in a grid box in each 5-yr period, and a value of 40% (light blue) represents the presence of at least 15% multiyear sea ice in a grid box in 2 out of the 5 yr. As can be seen in the plots, the satellite-derived data have a much finer resolution (12.5 km × 12.5 km) than the model (1°, which, averaged over the Arctic, translates to about 65 km × 30 km).

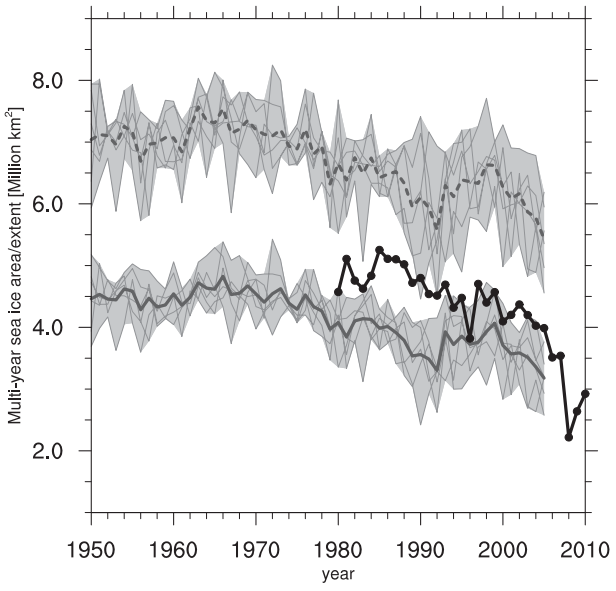

FIG. 7. CCSM4 ensemble mean multiyear (>1 yr) sea ice area (solid gray line) and extent (dashed gray line) over time, compared with the multiyear ice extent calculated from Lagrangian tracking of sea ice in satellite data (black line with round markers; see text for references and details on the method). The sea ice area and extent of individual ensemble members (thin gray lines), and the range of sea ice area and extent covered by the six ensemble members (gray shading) are also shown. The multiyear sea ice extent ignores areas with multiyear sea ice concentrations of less than 15%. Furthermore, the CAA, Hudson Bay, and Baffin Bay are masked out in the model results to match the coverage of the data product.

[December–March (DJFM)] shows the standard large-scale features, like the Beaufort Gyre and the Transpolar Drift Stream, that are also seen in the pathfinder data. The simulated ice speeds in the Arctic, however, are overall too large and show a wider distribution of speeds than those seen in the pathfinder data (not shown). Furthermore, compared to the satellite data the simulated Beaufort Gyre circulation is weaker and the center is shifted toward the East Siberian Sea. The Beaufort Gyre is even less prominent in the annual mean sea ice motion field (not shown), mainly because of a complete absence of an anticyclonic circulation cell between April and November (see Figs. 8c–f). This is mainly due to a strong underprediction of the strength of the Beaufort high in the CCSM4 simulations [see Fig. 4 and the description of the sea level pressure bias in de Boer et al. (2012)].

In addition to the bias in the climatological sea ice motion field, the six ensemble members have different temporal variations of important modes of atmospheric conditions than in the observed 1981–2005 record. If we take the Arctic Oscillation index for DJFM from the National Oceanic and Atmospheric Administration as proxy for the atmospheric conditions that affect sea ice motion, we find that 16% of the winters between 1981 and 2005 had a DJFM Arctic Oscillation (AO) index that is larger than one standard deviation of the mean, and 12% of the years had a DJFM AO index that is one standard deviation smaller than the mean. Applying the same one standard deviation cutoff for the 150 yr from the six ensemble runs for 1981–2005, 22% of the years were strongly AO positive and 15% were strongly AO negative. Given that the AO distribution is non-Gaussian, a more consistent way to compare the velocity fields is to use composites of strong AO-positive and AO-negative years from both the satellite record and the CCSM4 simulations (see Fig. 9). It can be seen that because of the larger percentage of strong AO-positive years in the ensemble mean than in the observational record, the ensemble mean for 1981–2005 also shows a more cyclonic circulation than the average 1981–2005 satellite-derived ice motion (compare Figs. 8a,b with Fig. 9). Furthermore, Fig. 9 shows that, despite the overall too-weak Beaufort Gyre, the CCSM4 shows the correct qualitative changes in the winter circulation regimes in the Arctic Ocean (described by Proshutinsky and Johnson 1997) from a more anticyclonic circulation with a stronger Beaufort Gyre during negative AO periods (Figs. 9c,d) to a more cyclonic circulation with a weaker Beaufort Gyre and a poleward shift of the TDS during AO-positive periods (Figs. 9a,b).

e. Melt-onset and freeze-up dates

Changes in the state of the Arctic sea ice cover are intricately linked to changes in the annual cycle of sea ice growth and decay, which is related to changes in the seasonal timing of the onset of summer melt and the initiation of fall freeze up. Hence, it is important to determine how well the model captures the seasonal timing of these melt season characteristics. To this end, we compare the model results with satellite passive microwave-derived melt-onset and freeze-up dates from Markus et al. (2009). This dataset indicates the day at which continuous melting and freezing at the surface begins, based on an algorithm that relies on the sensitivity of passive microwave brightness temperatures to liquid water content in the snow–ice cover [see Markus et al. (2009) for details on the method].

In the CCSM4, we use daily model output from the one ensemble member that has this high-frequency output. Melt onset is defined as the date at which the gridcell-averaged ice surface (or overlying snow) temperature increases above −1°C and freeze up is defined as the date when the surface temperature decreases below −1°C. In marginal ice zone regions, this freeze-up date is the time after ice formation is initiated so that the ice surface temperature drops below −1°C. Other measures of melt

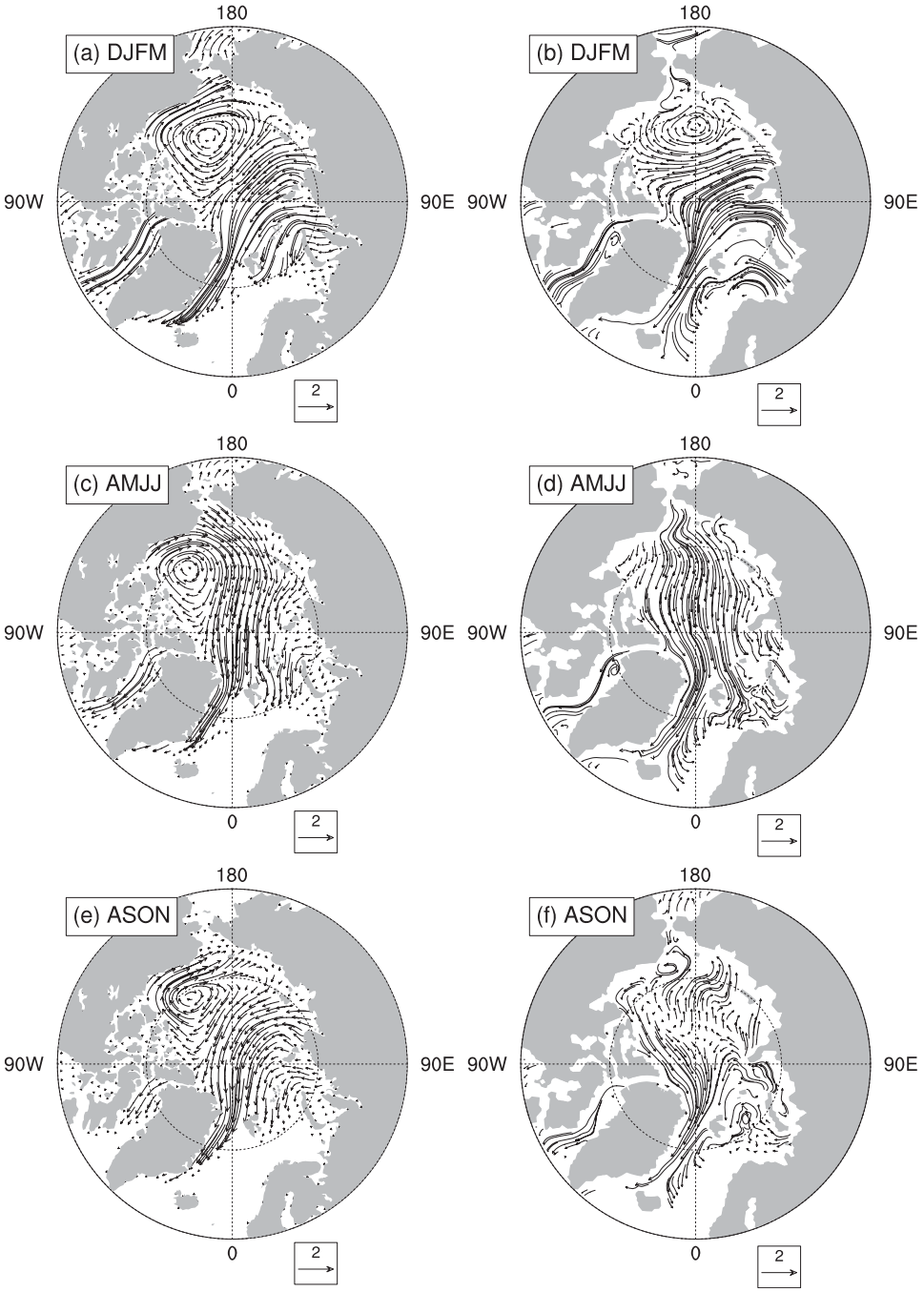

FIG. 8. Sea ice motion field for different seasons [DJFM, April–July (AMJJ), August–November (ASON)] from (a),(c),(e) satellite data (Fowler 2003) and (b),(d),(f) the CCSM4 ensemble mean averaged over 1981–2005. A reference vector (cm s^{-1}) is given in the plots. The vectors are represented using a curved polyline tangent to the instantaneous flow in the neighborhood of the grid point.

onset and freeze up in the model were also considered, including the first date of snow melting and the date of the initiation of ice formation within open water. We choose to use the surface temperature criteria here because of its simplicity. However, the model results are quite sensitive to the exact definition used for melt onset and freeze up, as also seen for several of the other fields (e.g., multiyear ice fraction and ice thickness). This again highlights the difficulties in comparing satellite-derived products to climate model output, where not only resolution and spatial

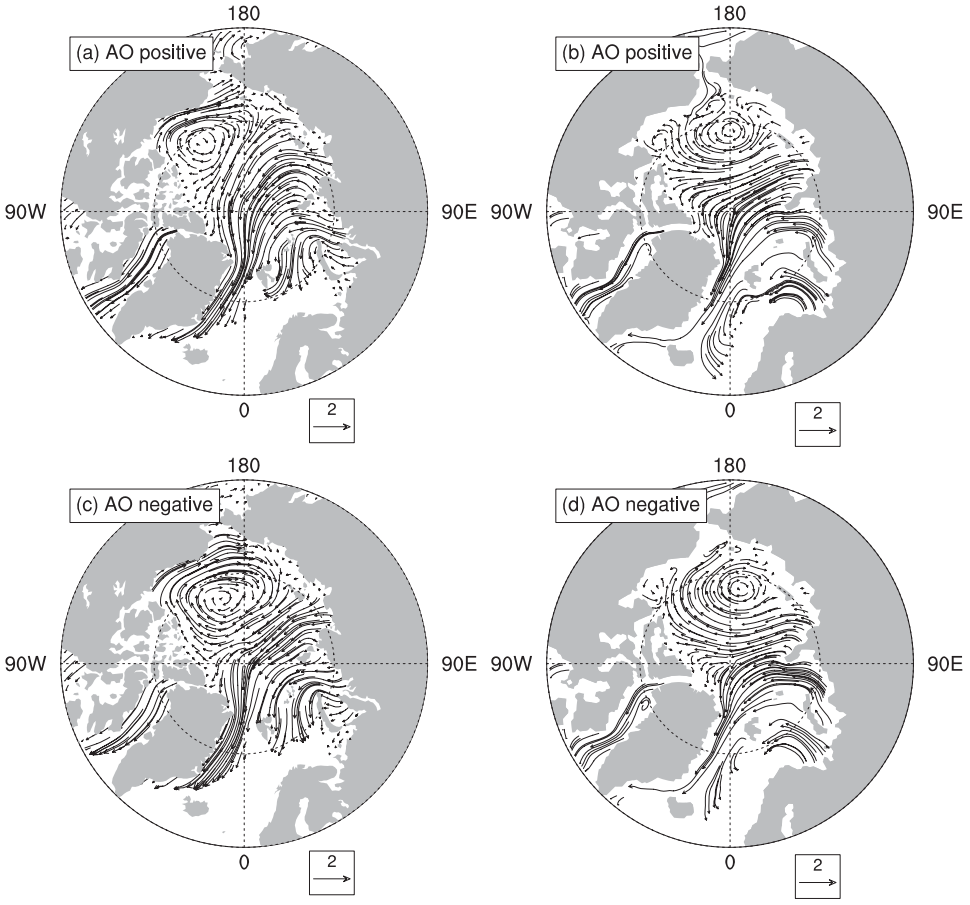

FIG. 9. Composites of the DJFM ice motion field for (a),(b) positive and (c),(d) negative DJFM AO index years from the (a),(c) satellite data and (b),(d) the CCSM4. As in Fig. 8, the vectors are represented using a curved polyline tangent to the instantaneous flow in the neighborhood of the grid point and a reference vector is given in each plot.

sampling are problematic, but the definitions of certain characteristics are also necessarily different. Hence, a qualitative comparison of the timing of melt onset and freeze up is most appropriate.

As can be seen in Fig. 10, melt-onset dates are broadly similar between the model and observations. As is clear from the histogram (Fig. 10, right column), the model obtains earlier melt-onset dates over large areas. However, the discrepancy with the observations is only by a couple weeks, which is likely well within the uncertainty in the data–model comparison. On average, for the 70°–85°N region, the modeled and observed melt onset differ by only a few days. The fall freeze-up date is also qualitatively similar between the model and observations. The modeled distribution is generally offset earlier by 5–10 days compared to the satellite data. The discrepancy in freeze up is larger than that for melting, with modeled freeze up averaging about 18 days earlier for the 70°–85°N area. Using an open water freezing criteria for freeze up (not shown), modeled values differ on average from the satellite freeze up by only 1 day. The melt season length (defined as the freeze up minus the onset date) is also in good agreement with the satellite-derived observations both in magnitude and spatial structure. The modeled melt season length averages 78 days compared to 90 days in the satellite observations for the 70°–85°N region.

4. Arctic Ocean

In contrast to the previous section about Arctic sea ice (section 3), where several satellite-derived datasets allowed us to constrain the CCSM4 simulation rather well, despite difficulties resulting from different definitions of variables, oceanographic data for the Arctic Ocean are still rather sparse and exist mainly in the form of climatological fields along cruise tracks and of mooring data that generally do not span more than 10 yr. Consequently,

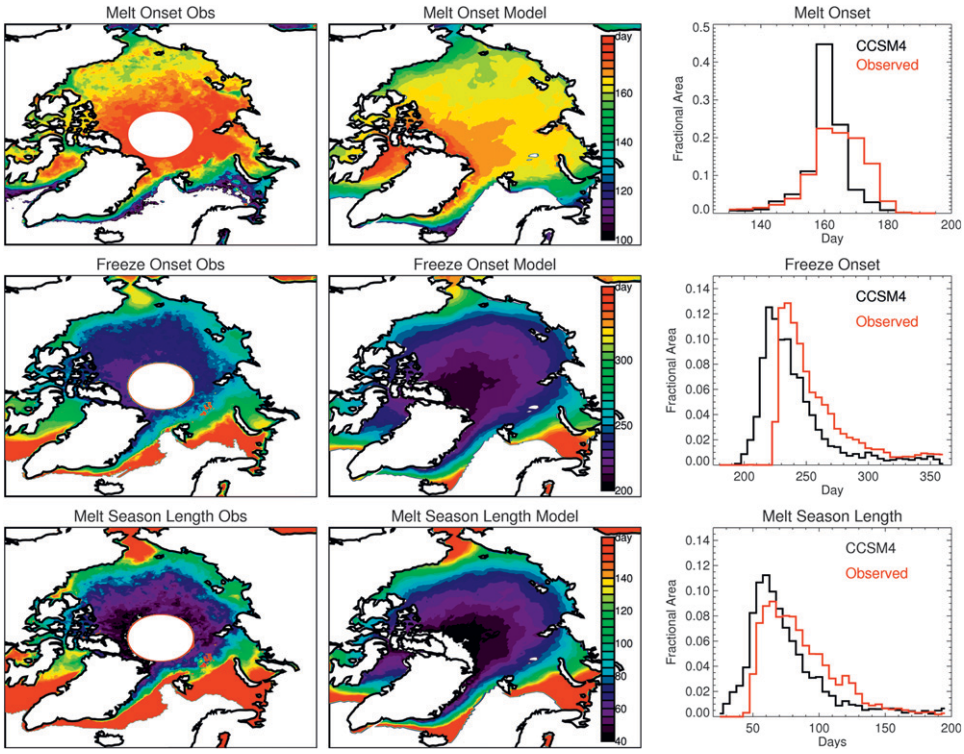

FIG. 10. (top to bottom) Melt onset, freeze onset, and melt season length from (left) satellite data and (right) one of the CCSM4 ensemble members (the only one with daily output) averaged over 1979–2000. The histogram shows the frequency distribution of melt-onset, freeze-up, and melt season length dates between 70° and 85°N in both the satellite data and the CCSM4.

we cannot assess how well the CCSM4 captures the temporal variability of oceanic properties in the Arctic Ocean. We can, however, use the climatological fields and the various flux measurements reported in the literature to establish how well the CCSM4 captures the climatological features of the Arctic water masses and the volume, heat, and freshwater fluxes both in and out of the Arctic. This is done in the following subsections (sections 4a–b).

a. Water masses and vertical structure

The simulated surface salinity in the central Arctic (80°–90°N) is 0.35 psu too large compared to the Polar Science Center Hydrographic Climatology version 2 (PHC2) data (Steele et al. 2001), whereas the simulated salinities between 50 m and 350 m depth in the central Arctic are between 0.1 and 0.2 psu too fresh, with good agreement below 350 m (see Fig. 11b). The vertical temperature structure, on the other hand, is fairly well captured in the top 250 m, but below that the simulated temperatures are generally too warm, with the temperature maximum located 400 m too deep and very little cooling below it (see Fig. 11a). This is caused by a strong bias in the simulation of the Atlantic water (AW) layer in the Arctic, which is generally too warm and has its core (defined as the subsurface temperature maximum) about 400 m deeper than that shown by the PHC2 data. The largest differences in the simulated AW core temperatures (AWCTs) compared to the PHC2 data occur along the pathways of AW inflows, with cooler (by 0.25°–1°C) simulated temperatures of the inflowing Fram Strait AW branch and warmer temperatures simulated in the Barents and Kara Seas (see Fig. 12). In the Amerasian Basin, the CCSM4 overestimates AWCT by 0.25°–0.5°C compared to the PHC2 data, indicating that the AW layer is not cooling as much as it should while circulating the Arctic Ocean.

An initial analysis of the temporal evolution of the temperature profile and of the age of the water mass below 1000 m suggests that the warm bias in the deep Arctic Ocean is caused by the lack of deep convection in the Arctic Ocean, so that the temperatures in the deep basin slowly increase over time. This deep convection should take place on the shelves, associated with the brine rejection from sea ice formation, and should lead to the sinking of cold and salty water to the deep Arctic Ocean, leading to a cooling of the deep water in the Arctic. Because the details of the bathymetry of the

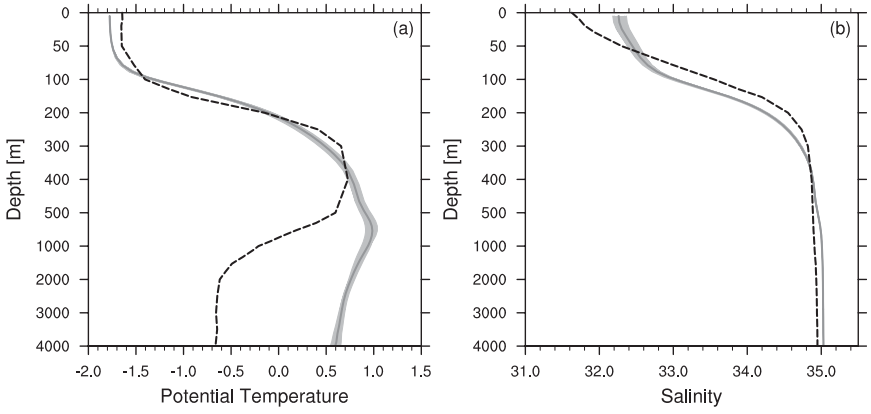

FIG. 11. (a) Potential temperature (°C) and (b) salinity (psu) profiles in the central Arctic (80°–90°N) from the PHC2 data (black dashed; Steele et al. 2001) and the 1981–2005 CCSM4 ensemble mean (dark gray). The ensemble spread is shown as light gray shading around the ensemble mean. Note the irregular *y* axis, which emphasizes the top 500 m.

shelves are important for this process, the current resolution of the CCSM4 is likely not high enough to capture this process. Further analysis of the detailed causes for the bias in the AW circulation in the Arctic, however, requires more work and is not the objective of this paper.

Despite these biases in the AW core depth, the circulation at the AW core depth in the CCSM4 agrees remarkably well with observations of intermediate AW pathways (Rudels et al. 1994; Dmitrenko et al. 2008; Polyakov et al. 2004) and follows the bathymetry of the Arctic Ocean, keeping shallow regions to the right. Specifically, the CCSM4 accurately depicts (i) the inflow of AW from the Fram Strait and the Barents and Kara Seas, (ii) the cyclonic boundary current around the marginal seas, (iii) the topographically steered cyclonic gyre in the Canadian Basin, (iv) the return flow of AW along the Lomonosov Ridge, and (v) the return Atlantic Current west and north of Svalbard (see Fig. 12).

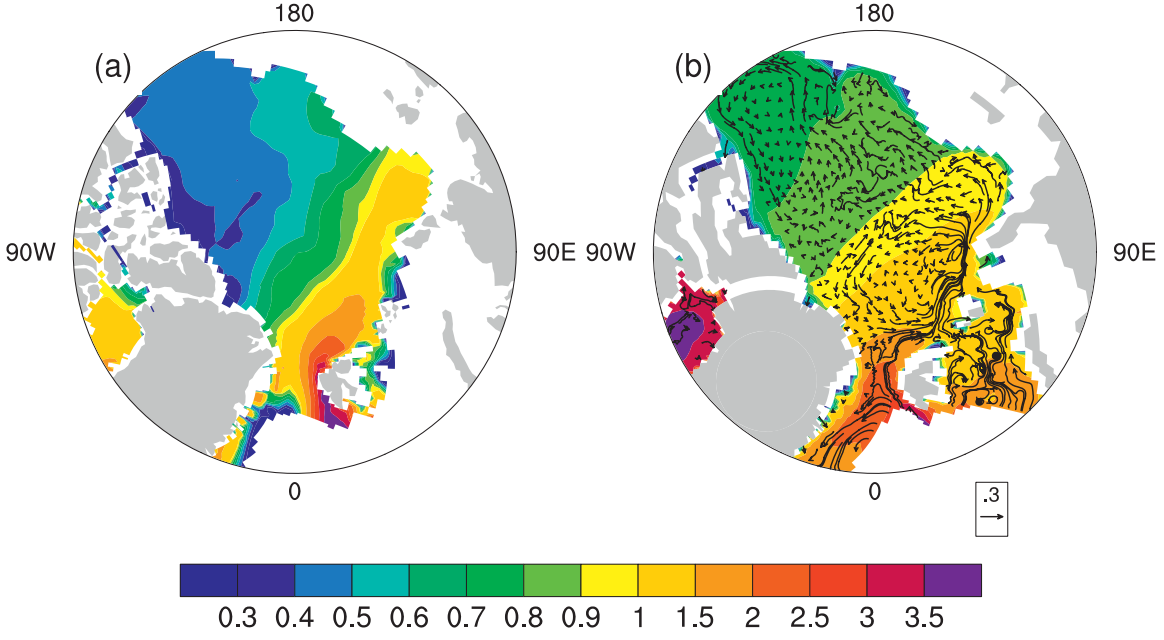

FIG. 12. Temperature (°C) at the Atlantic water core depth (defined as the maximum temperature in the subsurface water column) from (a) the PHC2 climatology (Steele et al. 2001) and (b) the ensemble mean of the twentieth-century CCSM4 simulation for 1981–2005. In addition, the model velocity field at the Atlantic water core depth (cm s^{-1}) is also shown, which reproduces the observed circulation features; that is, the cyclonic boundary circulation and a return flow of AW along the Lomonosov Ridge as well as north of the Fram Strait.

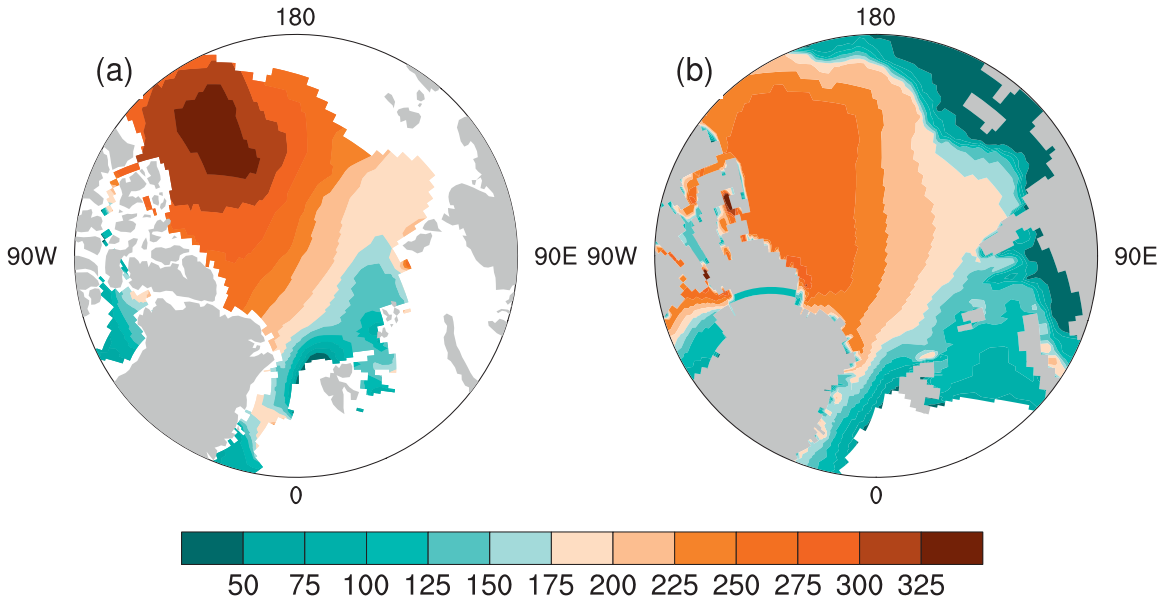

FIG. 13. Upper Atlantic water depth (m), with the depth of the upper Atlantic water defined as the depth of the 0°C isotherm, from the (a) PHC2 climatology (Steele et al. 2001) and (b) CCSM4 ensemble mean for 1981–2005.

In contrast to the AW core depth, the upper Atlantic water depth (defined as the 0°C isotherm) is well simulated compared to the PHC2 temperature data (see Fig. 13). The simulated upper AW depth in the Amerasian Basin is approximately 25–100 m shallower than that of observations, with the largest differences occurring near the observational maximum in the Beaufort Sea and extending into the East Siberian Sea. The poor location of the simulated maximum north of Ellesmere Island (instead of in the Beaufort Sea) occurs in response to the weak Beaufort Gyre discussed earlier. Apart from the location of the maximum, the CCSM4 simulated depth of the upper AW layer is reasonable when compared to observational data.

b. Fluxes in and out of the Arctic Ocean

The exchange between the Arctic Ocean and the North Atlantic through the Fram Strait includes a northward-flowing West Spitsbergen Current and a southward-flowing East Greenland Current. The simulated mass transport in these currents is smaller than that observed, with an inflow of 1.3 Sv (1 Sv $\equiv 10^6$ m^3 s^{-1}) and an outflow of 3.1 Sv through the Fram Strait compared to an observed volume flux of about 12 Sv northward and 14 Sv southward (Schauer et al. 2008). The net southward volume flux of 1.8 Sv through the Fram Strait, however, is comparable with the observational net southward volume flux of 2 Sv (Schauer et al. 2008). The volume fluxes through the Barents Sea Opening (BSO) and the Bering Strait are also comparable with the observations (see Table 2). These exchanges with the North Atlantic and North Pacific are important, because the inflow of Atlantic water supplies heat and salty water to the Arctic, the import of Pacific water supplies heat and FW to the Arctic, and the export of surface water from the Arctic supplies FW to the North Atlantic. Hence, while the correct magnitudes of these volume fluxes are important, correct heat and FW fluxes are arguably even more important. To compare the simulated AW and heat fluxes between the North Atlantic and Arctic Oceans with the observations, AW is defined using temperature cutoffs of $T > 1$°C for the Fram Strait, and $T > 2$°C for the BSO. All heat transports are calculated with a reference temperature of −0.1°C, and all FW transports use a reference salinity of 34.8.

We find that the CCSM4 is not able to fully resolve the West Spitsbergen Current in the Fram Strait along the shelf, resulting in extremely low AW volume fluxes into the Arctic through this channel (see Table 2). While the inflowing AW temperature is simulated at 2.2°C, well within the 1.9°–2.8°C observational range reported by Schauer et al. (2008), the resultant inward heat transport is only 11.4 TW, because of the weak simulated volume flux of 1.3 Sv. The simulated BSO AW transports are more accurate (see Table 2), with a simulated inflow of AW of 3.7 Sv, which is an overestimation of 0.6–2 Sv when compared to observations (Smedsrud et al. 2010; Ingvaldsen et al. 2004; Loeng et al. 1997). The simulated temperature of the inflowing AW is 4.9°C, in good agreement with the observational range of 4.3°–6.4°C reported by Smedsrud et al. (2010). The resultant AW heat transport into the Arctic is 76.1

TABLE 2. Climatological Arctic oceanic heat and volume fluxes for 1981–2005 from the twentieth-century simulations with the CCSM4 and from available observations. Shown is the ensemble mean of six CCSM4 simulations. Heat fluxes are calculated relative to −0.1°C. AW heat fluxes only consider water with temperatures either larger than or equal to 1.0°C for the Fram Strait and 2.0°C for the BSO, while heat fluxes are calculated relative to −0.1°C. Units: heat fluxes, TW, volume fluxes, Sv, and temperature, °C.

Fluxes	CCSM4	Observations	References
Fram Strait			
Volume flux (net/in/out)	−1.8/1.3/−3.1	−2/12/−14	Schauer et al. (2008)
		−1.9/11.64/−13.5	Fahrbach (2006)
Heat flux (net/in/out)	10.3/11.4/−1.1	36.8/58.6/−21.8	Fahrbach (2006)
AW volume flux (in)	1.2	5–7	Schauer et al. (2008)
		9–10	Schauer et al. (2004)
		2–8	Simonsen and Haugan (1996)
AW temperature (in)	2.2	1.9–2.8	Schauer et al. (2008)
AW heat flux (in)	11.3	26–50	Schauer et al. (2008)
		18–67	Simonsen and Haugan (1996)
Barents Sea Opening			
Volume flux (net/in/out)	2.3/3.8/−1.4	2.0/3.2/−1.2	Smedsrud et al. (2010)
Heat flux (net/in/out)	54.7/76.2/−21.5	73/86/−12	Smedsrud et al. (2010)
AW volume flux (in)	3.7	2	Smedsrud et al. (2010)
		1.3–1.7	Ingvaldsen et al. (2004)
		3.1	Loeng et al. (1997)
AW temperature (in)	4.9	4.3–6.4	Smedsrud et al. (2010)
		4.7–6.2	Simonsen and Haugan (1996)
AW heat flux (in)	76.1	49.7	Smedsrud et al. (2010)
		62–82	Simonsen and Haugan (1996)
Bering Strait			
Volume flux (net)	1.1	0.8	Woodgate and Aagaard (2005)
Nares Strait			
Volume flux (net)	−1.5	0.57 ±0.09	Münchow and Melling (2008)
Barrow Strait			
Volume flux (net)	−0.3	0.7 ±0.3	Prinsenberg et al. (2009)

TW, which is larger than the most recent measurements of 49.7 TW reported by Smedsrud et al. (2010), but within the 62–81-TW observational range provided in Simonsen and Haugan (1996). Hence, given the large interannual variability of the heat flux into the Arctic Ocean and the still-limited length of observations, we conclude that the simulated BSO AW heat fluxes are likely biased high, but are in better agreement with observations than the heat flux into the Arctic Ocean through the Fram Strait.

The simulated FW budget of the Arctic Ocean is in reasonable agreement with the observations (see Table 3), with the largest bias being a too-large FW input through runoff, a too-large liquid FW export through the BSO, and a too-small liquid FW export through Fram Strait. However, it is important to note that the observational values of the FW fluxes, especially in the ocean, also have large uncertainties and are based on short time series [often less than 10 yr; see Serreze et al. (2006) and Dickson et al. (2007) for a summary of our current knowledge about the Arctic FW fluxes].

Compared to the CCSM3, the FW budget of the CCSM4 is in overall better agreement with the observations, largely due to the opening of the Nares Strait in the CCSM4, which leads to much more FW export through the CAA than before and reduces the overly large liquid FW export through the Fram Strait that was seen in the CCSM3 [see Holland et al. (2006c) and Jahn et al. (2010) for detailed discussions of the FW fluxes and budget in the CCSM3]. As a consequence, the simulated FW transports east (through the Fram Strait and the BSO) and west (through the Barrow and Nares Straits) of Greenland in the CCSM4 are in good agreement with the observations. However, compared to the limited observations that are available (Melling 2004; Prinsenberg and Hamilton 2005; Münchow et al. 2006; Münchow and Melling 2008; Rabe et al. 2010), the split between the volume and FW export through Nares and Barrow Straits is likely not correctly simulated by the model, with a too-large volume and FW flux through Nares Strait (−1.5 Sv and −2410 $km^3\ yr^{-1}$, respectively) and a too-small volume and FW flux through Barrow Strait (−0.3 Sv and −908 $km\ yr^{-1}$, respectively). Compared to most IPCC Fourth Assessment Report (AR4) climate models (Solomon et al. 2007), however, having the correct total FW export east and west of Greenland in a fully coupled global climate model is a great improvement, because most climate models used for the last

TABLE 3. Climatological Arctic Ocean FW budget for 1981–2005 from the twentieth-century simulations with the CCSM4 and from observations. Shown is the ensemble mean of six CCSM4 simulations. All observational values are taken from Serreze et al. (2006), except for the Bering Strait sea ice flux, which is based on Woodgate and Aagaard (2005). Units: FW fluxes, $km^3\ yr^{-1}$. All fluxes are net annual mean fluxes through a channel, combining negative and positive fluxes through a strait, where applicable. All oceanic fluxes are calculated over the full depth of the water column at the boundaries. FW fluxes are calculated relative to a reference salinity of 34.8, with negative numbers indicating FW sinks for the Arctic Ocean and positive numbers indicating FW sources.

FW fluxes	CCSM4	Observations
River runoff	4156	3200
Net precipitation	2456	2000
Bering Strait solid FW	161	100
CAA solid FW	−405	−160
Fram Strait solid FW	−2980	−2300
Barents Sea Opening solid FW	−103	—
Bering Strait liquid FW	2999	2500
CAA liquid FW	−3318	−3200
Fram Strait liquid FW	−1609	−2660
Barents Sea Opening liquid FW	−865	−90
Net	493	−610

IPCC report did not have any open channels in the CAA, and hence no FW export west of Greenland [see Holland et al. (2007) for a comparison of the FW budget of several AR4 GCMs]. Having realistic FW fluxes on the eastern and western sides of Greenland can be of critical importance for the simulation of deep-water formation in the North Atlantic, as seen, for example, in a paleostudy of the last glacial inception (Jochum et al. 2012).

The liquid FW content in the CCSM4 ensemble mean for 1981–2005 is 86 371 km^3 (relative to 34.8 and integrated from the surface to 250-m depth), which is somewhat larger than the observational estimate of 74 000 $\pm$7400 km^3 derived from the climatological PHC2 data by Serreze et al. (2006). Because of the displacement of the Beaufort Gyre toward the East Siberian Sea (also section 3), the simulated FW storage maximum is more elongated compared to the quasi-circular FW maximum in the PHC data (Fig. 14). This bias in the Beaufort Gyre region is also clearly visible in the annual mean surface ocean velocity (see vector field in Fig. 14b). In contrast to the sea ice motion, where the anticyclonic circulation vanishes during spring, summer, and fall, the ocean circulation in the Canadian Basin stays anticyclonic year-round, resulting from a weaker response of the ice-covered surface ocean to the annual cycle of the wind forcing (not shown). As shown for the sea ice motion, the Beaufort Gyre circulation in the upper ocean also shows changes in its strength and location in response to atmospheric forcing. The resultant changes in the freshwater storage, however, tend to be smaller than those seen in the CCSM3.

5. Summary

Using the available data for the Arctic sea ice cover and the Arctic Ocean, we showed that the late-twentieth-century simulations from the CCSM4 capture many of the important properties of the Arctic sea ice and ocean well. Specifically, we have shown that the simulated spatial sea ice concentration, sea ice extent, multiyear sea ice concentration, sea ice thickness pattern, and melt season length are well captured by the CCSM4. The observed decreasing trend in the September Arctic sea ice extent over 1981–2005 is within the spread of the ensemble members. The simulated trends over this relatively short period are, however, strongly affected by internal variability, and we found that five ensemble members are just enough to detect the negative trend in the ensemble mean sea ice extent over this period. From the individual ensemble members, only four out of the six ensemble members show a significant negative sea ice extent trend over 1981–2005, with one ensemble member showing a larger trend than that observed, and three ensemble members showing smaller trends than those observed. Over longer periods (i.e., 1950–2005), the spread in the sea ice extent trend in the different ensemble members is reduced, and all ensemble members, as well as the ensemble mean, show a decreasing trend in the sea ice extent. We also found that the decrease of the old and thick ice is very different between the individual ensemble members and that trends in the sea ice extent, which do not account for open water areas within the ice pack, are much more variable between individual ensemble members than trends in the sea ice area. Because of the still relatively short time series of the satellite-derived sea ice extent, and the strong influence of internal variability on the simulated sea ice extent trends, we speculate that the observed trend has a strong imprint of internal variability that has enhanced the summer sea ice loss. Furthermore, because of the imprint of internal variability it is important to not just compare the observed sea ice trend with the ensemble mean or a multimodel ensemble mean, but to also compare it with individual ensemble members, because the observed trend is representative of a single realization with contributions from both internal variability and forced change.

The largest bias in the sea ice simulation of the CCSM4 is found in the sea ice motion field, which shows a displaced and too-weak Beaufort Gyre as well as unrealistic sea ice motion in all seasons except winter. This is caused by a strong bias in the sea level pressure over the Beaufort Sea (see de Boer et al. 2012), which also

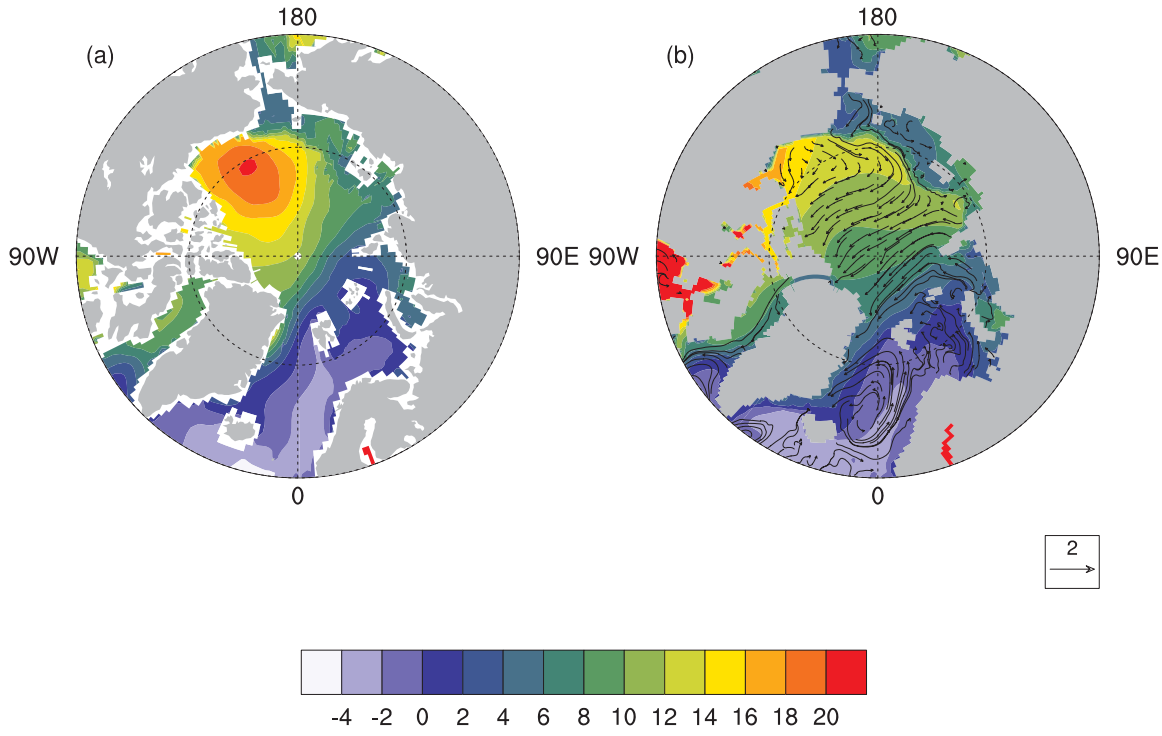

FIG. 14. Climatological liquid FW column (m) from (a) PHC 2 (Steele et al. 2001) and (b) the CCSM4 ensemble mean (for 1981–2005). The liquid FW content is calculated for the top 250 m and relative to a reference salinity of 34.8. In (b), the simulated ensemble mean 1981–2005 ocean surface velocity (cm s^{-1}) is also shown.

leads to a too-weak and displaced oceanic Beaufort Gyre circulation. In contrast to the sea ice, the Beaufort Gyre circulation is present in all seasons in the upper ocean. As a result of the shifted Beaufort Gyre, the FW content maximum is more elongated than that observed. Despite the bias in the mean state of the Beaufort Gyre, the upper ocean and sea ice motion fields show changes in the strength of the Beaufort Gyre in response to changes in the atmospheric forcing that are qualitatively similar to the observations.

We furthermore showed that the simulated temperature of the inflowing Atlantic water has realistic temperatures; however, because of too-low volume inflow, especially in the Fram Strait, the resulting heat flux into the Arctic Ocean is too low compared to that of the observations. The AW layer in the Arctic Ocean has a realistic upper depth; however, the maximum AW core temperatures are located 400 m deeper than that shown by the observations. In addition, the deep Arctic Ocean is too warm because of a lack of deep convection in the Arctic Ocean that would supply colder water. The simulated FW transports both in and out of the Arctic are in reasonable agreement with the observations, with realistic FW fluxes east and west of Greenland, despite biases in the distribution between the Nares and Barrow Straits and between the Fram Strait and the BSO.

Overall, we conclude that the CCSM4 reasonably simulates the important properties of the Arctic Ocean, and that its performance in the Arctic Ocean has generally improved compared to the CCSM3. The most important biases to keep in mind for future work with the CCSM4 in the Arctic are the problems with the sea ice motion between spring and fall, and the displaced and too-weak Beaufort Gyre, which occur as the result of a bias in the sea level pressure field over the Arctic. On the other hand, the ability of the CCSM4 to simulate the observed rapid changes in the Arctic sea ice cover since the beginning of the satellite era is promising for the ability to use ensemble simulations of the CCSM4 for studies of future changes in the Arctic sea ice.

Acknowledgments. Special thanks to Igor V. Polyakov (IARC) and Uma S. Bhatt (IARC) for their advice on the analysis of the Atlantic water properties, to Clara Deser (NCAR) and Ron Kwok (JPL) for discussions, and to the reviewer and editor for comments on earlier versions of the manuscript. Alexandra Jahn was supported through a Postdoctoral Fellowship from the Advances Study Program at NCAR. Kara Sterling was supported in part by a grant of HPC resources from the Arctic Region Supercomputing Center at the University of Alaska Fairbanks (UAF) as part of the

Department of Defense High Performance Computing Modernization Program and by the International Arctic Research Center (IARC), UAF. Marika Holland acknowledges support through NSF OPP-0902068. Cecilia M. Bitz acknowledges support through NSF Grant ARC-0909313. Julienne Stroeve acknowledges funding from NASA under Grants NNG04GO51G and NNG06GB26G. Elizabeth Hunke and William Lipscomb acknowledge funding from the Biological and Environmental Research division of the U.S. Department of Energy Office of Science; Los Alamos National Laboratory is operated by the National Nuclear Security Administration of the U.S. Department of Energy under Contract DEAC52-06NA25396. The CESM project is supported by the National Science Foundation and the Office of Science (BER) of the U.S. Department of Energy. Computing resources were provided by the Climate Simulation Laboratory at NCAR's Computational and Information Systems Laboratory (CISL), sponsored by the National Science Foundation and other agencies. The CMIP5 simulations used in this research were enabled by CISL computer and storage resources. Bluefire, a 4064-processor IBM Power6 resource with a peak of 77 TeraFLOPS provided more than 7.5 million computing hours, the GLADE high-speed disk resources provided 0.4 PB of dedicated disk, and CISL's 12-PB HPSS archive provided over 1 PB of storage in support of the research project.

REFERENCES

Agnew, T., and S. Howell, 2003: The use of operational ice charts for evaluating passive microwave ice concentration data. *Atmos.–Ocean,* **41,** 317–331, doi:10.3137/ao.410405.

Arctic Climate Impact Assessment, 2005: *Impacts of a warming Arctic: Arctic Climate Impact Assessment 2005*. Cambridge University Press, 1042 pp.

Arnell, N. W., 2005: Implications of climate change for freshwater inflows to the Arctic Ocean. *J. Geophys. Res.,* **110,** D07105, doi:10.1029/2004JD005348.

Bitz, C. M., and W. H. Lipscomb, 1999: An energy-conserving thermodynamic model of sea ice. *J. Geophys. Res.,* **104** (C7), 15 669–15 677.

——, P. G. Gent, R. A. Woodgate, M. M. Holland, and R. Lindsay, 2006: The influence of sea ice on ocean heat uptake in response to increasing CO_2. *J. Climate,* **19,** 2437–2450.

Briegleb, B. P., and B. Light, 2007: A Delta-Eddington multiple scattering parameterization for solar radiation in the sea ice component of the Community Climate System Model. National Center for Atmospheric Research Tech. Note 472+STR, 100 pp.

Cavalieri, D. J., C. L. Parkinson, P. Gloersen, J. C. Comiso, and H. J. Zwally, 1999: Deriving long-term time series of sea ice cover from satellite passive-microwave multisensor data sets. *J. Geophys. Res.,* **104** (C7), 15 803–15 814.

Comiso, J., 1999, updated 2008: Bootstrap sea ice concentrations from NIMBUS-7 SMMR and DMSP SSM/I, 1979–2007. National Snow and Ice Data Center, Boulder, CO, digital media. [Available online at http://nsidc.org/data/docs/daac/nsidc0079_bootstrap_seaice.gd.html.]

Danabasoglu, G., S. Bates, B. P. Briegleb, S. R. Jayne, M. Jochum, W. G. Large, S. Peacock, and S. G. Yeager, 2012: The CCSM4 ocean component. *J. Climate,* **25,** 1361–1389.

de Boer, G., W. Chapman, J. Kay, B. Medeiros, M. D. Shupe, S. Vavrus, and J. Walsh, 2012: A characterization of the present-day Arctic atmosphere in CCSM4. *J. Climate,* in press.

Deser, C., R. Tomas, M. Alexander, and D. Lawrence, 2010: The seasonal atmospheric response to projected Arctic sea ice loss in the late twenty-first century. *J. Climate,* **23,** 333–351.

——, A. Phillips, V. Bourdette, and H. Teng, 2011: Uncertainty in climate change projections: The role of internal variability. *Climate Dyn.,* **38,** 527–546.

Dickson, R., B. Rudels, S. Dye, M. Karcher, J. Meincke, and I. Yashayaev, 2007: Current estimates of freshwater flux through Arctic and subarctic seas. *Prog. Oceanogr.,* **73** (3–4), 210–230, doi:10.1016/j.pocean.2006.12.003.

Dmitrenko, I. A., and Coauthors, 2008: Toward a warmer Arctic Ocean: Spreading of the early 21st century Atlantic Water warm anomaly along the Eurasian Basin margins. *J. Geophys. Res.,* **113,** C05023, doi:10.1029/2007JC004158.

Durner, G. M., and Coauthors, 2009: Predicting 21st-century polar bear habitat distribution from global climate models. *Ecol. Monogr.,* **79,** 25–58, doi:10.1890/07-2089.1.

Fahrbach, E., 2006: ASOF-N: Arctic-subarctic ocean flux array for European climate: North. Final Report: 1 January 2003 to 31 March 2006, Alfred Wegener Institut für Polar- und Meeresforschung Tech. Rep., Contract EVK2-CT-2002-00139, 164 pp. [Available online at http://epic-reports.awi.de/2719/1/Fah2006h.pdf.]

Fetterer, F., K. Knowles, W. Meier, and M. Savoie, 2002, updated 2010: Sea ice index. National Snow and Ice Data Center, Boulder, CO, digital media. [Available online at http://nsidc.org/data/docs/noaa/g02135_seaice_index/.]

Fowler, C., 2003: Polar pathfinder daily 25 km EASE-grid sea ice motion vectors, 01/1981–12/2005. National Snow and Ice Data Center, Boulder, CO, digital media. [Available online at http://nsidc.org/data/nsidc-0116.html.]

——, W. Emery, and J. A. Maslanik, 2003: Satellite derived Arctic sea ice evolution, October 1978 to March 2003. *Trans. Geosci. Remote Sens. Lett.,* **1,** 71–74.

Gent, P. R., and Coauthors, 2011: The Community Climate System Model version 4. *J. Climate,* **24,** 4973–4991.

Giles, K. A., S. W. Laxon, and A. L. Ridout, 2008: Circumpolar thinning of Arctic sea ice following the 2007 record ice extent minimum. *Geophys. Res. Lett.,* **35,** L22502, doi:10.1029/2008GL035710.

Haas, C., A. Pfaffling, S. Hendricks, L. Rabenstein, J.-L. Etienne, and I. Rigor, 2008: Reduced ice thickness in Arctic Transpolar Drift favors rapid ice retreat. *Geophys. Res. Lett.,* **35,** L17501, doi:10.1029/2008GL034457.

Holland, M. M., C. M. Bitz, E. C. Hunke, W. H. Lipscomb, and J. L. Schramm, 2006a: Influence of the sea ice thickness distribution on polar climate in CCSM3. *J. Climate,* **19,** 2398–2414.

——, ——, and B. Tremblay, 2006b: Future abrupt reductions in the summer Arctic sea ice. *Geophys. Res. Lett.,* **33,** L23503, doi:10.1029/2006GL028024.

——, J. Finnis, and M. C. Serreze, 2006c: Simulated Arctic Ocean freshwater budgets in the twentieth and twenty-first centuries. *J. Climate,* **19,** 6221–6242.

——, ——, A. P. Barrett, and M. C. Serreze, 2007: Projected changes in Arctic Ocean freshwater budgets. *J. Geophys. Res.,* **112,** G04S55, doi:10.1029/2006JG000354.

——, C. M. Bitz, B. Tremblay, and D. A. Bailey, 2008: The role of natural versus forced change in future rapid summer Arctic ice loss. *Arctic Sea Ice Decline: Observations, Projections, Mechanisms, and Implications, Geophys. Monogr.,* Vol. 180, Amer. Geophys. Union, 133–150.

——, M. C. Serreze, and J. Stroeve, 2010: The sea ice mass budget of the Arctic and its future change as simulated by coupled climate models. *Climate Dyn.,* **34,** 185–200, doi:10.1007/s00382-008-0493-4.

——, D. A. Bailey, B. P. Briegleb, B. Light, and E. Hunke, 2012: Improved sea ice shortwave radiation physics in CCSM4: The impact of melt ponds and aerosols on Arctic sea ice. *J. Climate,* **25,** 1413–1430.

Hunke, E. C., and J. K. Dukowicz, 1997: An elastic-viscous-plastic model for sea ice dynamics. *J. Phys. Oceanogr.,* **27,** 1849–1867.

——, and W. H. Lipscomb, 2008: CICE: The Los Alamos sea ice model documentation and software user's manual version 4.1. Los Alamos National Laboratory Tech. Rep. LA-CC-06-012, 76 pp.

Ingvaldsen, R. B., L. Asplin, and H. Loeng, 2004: The seasonal cycle in the Atlantic transport to the Barents Sea during the years 1997–2001. *Cont. Shelf Res.,* **24,** 1015–1032, doi:10.1016/j.csr.2004.02.011.

Jahn, A., L. B. Tremblay, R. Newton, M. M. Holland, L. A. Mysak, and I. A. Dmitrenko, 2010: A tracer study of the Arctic Ocean's liquid freshwater export variability. *J. Geophys. Res.,* **115,** C07015, doi:10.1029/2009JC005873.

Jochum, M., A. Jahn, S. Peacock, D. Bailey, J. Fasullo, J. Kay, S. Levis, and B. Otto-Bliesner, 2012: True to Milankovitch: Glacial Inception in the new Community Climate System Model. *J. Climate,* in press.

Kay, J. E., M. M. Holland, and A. Jahn, 2011: Inter-annual to multi-decadal Arctic sea ice extent trends in a warming world. *Geophys. Res. Lett.,* **38,** L15708, doi:10.1029/2011GL048008.

Kwok, R., and G. F. Cunningham, 2008: ICESat over Arctic sea ice: Estimation of snow depth and ice thickness. *J. Geophys. Res.,* **113,** C08010, doi:10.1029/2008JC004753.

——, H. J. Zwally, and D. Yi, 2004: ICESat observations of Arctic sea ice: A first look. *Geophys. Res. Lett.,* **31,** L16401, doi:10.1029/2004GL020309.

——, G. F. Cunningham, M. Wensnahan, I. Rigor, H. J. Zwally, and D. Yi, 2009: Thinning and volume loss of the Arctic Ocean sea ice cover: 2003–2008. *J. Geophys. Res.,* **114,** C07005, doi:10.1029/2009JC005312.

Lawrence, D. M., and Coauthors, 2011: Parameterization improvements and functional and structural advances in version 4 of the Community Land Model. *J. Adv. Model. Earth Syst.,* **3,** M03001, doi:10.1029/2011MS000045.

Laxon, S., N. Peacock, and D. Smith, 2003: High interannual variability of sea ice thickness in the Arctic region. *Nature,* **425,** 947–949, doi:10.1038/nature02050.

Lipscomb, W. H., 2001: Remapping the thickness distribution in sea ice models. *J. Geophys. Res.,* **106** (C7), 13 989–14 000.

——, E. C. Hunke, W. Maslowski, and J. Jakacki, 2007: Ridging, strength, and stability in high-resolution sea ice models. *J. Geophys. Res.,* **112,** C03S91, doi:10.1029/2005JC003355.

Loeng, H., V. Ozhigin, and B. Adlandsvik, 1997: Water fluxes through the Barents Sea. *ICES J. Mar. Sci.,* **54,** 310–317.

Markus, T., and S. T. Dokken, 2002: Evaluation of late summer passive microwave Arctic sea ice retrievals. *IEEE Trans. Geosci. Remote Sens.,* **40,** 348–356, doi:10.1109/36.992795.

——, J. C. Stroeve, and J. Miller, 2009: Recent changes in Arctic sea ice melt onset, freezeup, and melt season length. *J. Geophys. Res.,* **114,** C12024, doi:10.1029/2009JC005436.

Maslanik, J. A., C. Fowler, J. Stroeve, S. Drobot, J. Zwally, D. Yi, and W. Emery, 2007: A younger, thinner Arctic ice cover: Increased potential for rapid, extensive sea-ice loss. *Geophys. Res. Lett.,* **34,** L24501, doi:10.1029/2007GL032043.

——, ——, ——, and W. Emery, 2011: Distribution and trends in Arctic sea ice age through spring 2011. *Geophys. Res. Lett.,* **38,** L13502, doi:10.1029/2011GL047735.

Maykut, G. A., and N. Untersteiner, 1971: Some results from a time-dependent thermodynamic model of sea ice. *J. Geophys. Res.,* **76** (6), 1550–1575.

McPhee, M. G., A. Proshutinsky, J. H. Morison, M. Steele, and M. B. Alkire, 2009: Rapid change in freshwater content of the Arctic Ocean. *Geophys. Res. Lett.,* **36,** L10602, doi:10.1029/2009GL037525.

Melling, H., 2004: Fluxes through the northern Canadian Arctic Archipelago. *ASOF Newsletter,* ASOF, No. 2, 3–7. [Available online at http://www.asof.awi.de/fileadmin/user_upload/Poster/NL2.pdf.]

Münchow, A., and H. Melling, 2008: Ocean current observations from Nares Strait to the west of Greenland: Interannual to tidal variability and forcing. *J. Mar. Res.,* **66,** 801–833.

——, ——, and K. K. Falkner, 2006: An observational estimate of volume and freshwater flux leaving the Arctic Ocean through Nares Strait. *J. Phys. Oceanogr.,* **36,** 2025–2041.

Polyakov, I. V., and Coauthors, 2004: Variability of the intermediate Atlantic water of the Arctic Ocean over the last 100 years. *J. Climate,* **17,** 4485–4497.

——, and Coauthors, 2005: One more step toward a warmer Arctic. *Geophys. Res. Lett.,* **32,** L17605, doi:10.1029/2005GL023740.

Prinsenberg, S. J., and J. Hamilton, 2005: Monitoring the volume, freshwater and heat fluxes passing through Lancaster Sound in the Canadian Arctic Archipelago. *Atmos.–Ocean,* **43,** 1–22.

——, ——, I. Peterson, and R. Pettipas, 2009: Observing and interpreting the seasonal variability of the oceanographic fluxes passing through Lancaster Sound of the Canadian Arctic Archipelago. *Influence of Climate Change on the Changing Arctic and Sub-Arctic Conditions,* J. C. J. Nihoul and A. G. Kostianoy, Eds., NATO Science for Peace and Security Series C: Environmental Security, Springer, 125–143.

Proshutinsky, A. Y., and M. A. Johnson, 1997: Two circulation regimes of the wind-driven Arctic Ocean. *J. Geophys. Res.,* **102** (C6), 12 493–12 514.

——, and Coauthors, 2009: Beaufort Gyre freshwater reservoir: State and variability from observations. *J. Geophys. Res.,* **114,** C00A10, doi:10.1029/2008JC005104.

Quadfasel, D., A. Sy, D. Wells, and A. Tunik, 1991: Warming in the Arctic. *Nature,* **350,** 385.

Rabe, B., A. Münchow, H. L. Johnson, and H. Melling, 2010: Nares Strait hydrography and salinity field from a 3-year moored array. *J. Geophys. Res.,* **115,** C07010, doi:10.1029/2009JC005966.

Rigor, I. G., and J. M. Wallace, 2004: Variations in the age of Arctic sea-ice and summer sea-ice extent. *Geophys. Res. Lett.,* **31,** L09401, doi:10.1029/2004GL019492.

Rothrock, D. A., Y. Yu, and G. A. Maykut, 1999: Thinning of the Arctic sea-ice cover. *Geophys. Res. Lett.,* **26,** 3469–3472.

Rudels, B., E. P. Jones, L. G. Anderson, and G. Kattner, 1994: On the intermediate depth waters of the Arctic Ocean. *The Polar Oceans and Their Role in Shaping the Global Environment: The Nansen Centennial Volume, Geophys. Monogr.,* Vol. 85, Amer. Geophys. Union, 33–46.

Schauer, U., E. Fahrbach, S. Osterhus, and G. Rohardt, 2004: Arctic warming through the Fram Strait: Oceanic heat transport from 3 years of measurements. *J. Geophys. Res.,* **109,** C06026, doi:10.1029/2003JC001823.

——, A. Beszczynska-Möller, W. Walczowski, E. Fahrbach, J. Piechura, and E. Hansen, 2008: Variation of measured heat flow through the Fram Strait between 1997 and 2006. *Arctic-Subarctic Ocean Fluxes,* R. R. Dickson, J. Meincke, and P. Rhines, Eds., Springer Science + Business Media, 65–85.

Serreze, M. C., and Coauthors, 2006: The large-scale freshwater cycle of the Arctic. *J. Geophys. Res.,* **111,** C11010, doi:10.1029/2005JC003424.

Simonsen, K., and P. M. Haugan, 1996: Heat budgets of the Arctic Mediterranean and sea surface heat flux parameterizations for the Nordic Seas. *J. Geophys. Res.,* **101** (C3), 6553–6576.

Smedsrud, L. H., R. Ingvaldsen, J. E. Ø. Nilsen, and Ø. Skagseth, 2010: Heat in the Barents Sea: Transport, storage, and surface fluxes. *Ocean Sci.,* **6,** 219–234, doi:10.5194/os-6-219-2010.

Smith, R., and Coauthors, 2010: The Parallel Ocean Program (POP) reference manual. Los Alamos National Laboratory Tech. Rep. LAUR-10-01853, 141 pp.

Solomon, S., D. Qin, M. Manning, Z. Chen, M. Marquis, K. Averyt, M. Tignor, and H. Miller, Eds., 2007: *Climate Change 2007: The Physical Science Basis*. Cambridge University Press, 996 pp.

Steele, M., R. Morley, and W. Ermold, 2001: PHC: A global ocean hydrography with a high-quality Arctic Ocean. *J. Climate,* **14,** 2079–2087.

Steffen, K., J. Comiso, K. S. Gemain, P. Gloersen, J. Key, and I. Rubenstein, 1992: The estimation of geophysical parameters using passive microwave algorithms. *Microwave Remote Sensing of Sea Ice,* F. D. Carsey, Ed., Amer. Geophys. Union, 201–228.

Stroeve, J., M. M. Holland, W. Meier, T. Scambos, and M. Serreze, 2007: Arctic sea ice decline: Faster than forecast. *Geophys. Res. Lett.,* **34,** L09501, doi:10.1029/2007GL029703.

——, M. Serreze, S. Drobot, S. Gearheard, M. Holland, J. Maslanik, W. Meier, and T. Scambos, 2008: Arctic sea ice extent plummets in 2007. *Eos, Trans. Amer. Geophys. Union,* **89,** 13, doi:10.1029/2008EO020001.

——, J. A. Maslanik, M. C. Serreze, I. Rigor, W. Meier, and C. Fowler, 2011: Sea ice response to an extreme negative phase of the Arctic Oscillation during winter 2009/2010. *Geophys. Res. Lett.,* **38,** L02502, doi:10.1029/2010GL045662.

Thorndike, A. S., D. S. Rothrock, G. A. Maykut, and R. Colony, 1975: Thickness distribution of sea ice. *J. Geophys. Res.,* **80** (C33), 4501–4513.

Tschudi, M., C. Fowler, J. Maslanik, and J. Stroeve, 2010: Tracking the movement and changing surface characteristics of Arctic sea ice. *IEEE J. Sel. Top. Appl. Earth Obs. Remote Sens.,* **3,** 546–540, doi:10.1109/JSTARS.2010.2048305.

Tucker, W. B., J. W. Weatherly, D. T. Eppler, L. D. Farmer, and D. L. Bentley, 2001: Evidence for rapid thinning of sea ice in the western Arctic Ocean at the end of the 1980s. *Geophys. Res. Lett.,* **28,** 2851–2854.

Vavrus, S., and D. Waliser, 2008: An improved parameterization for simulating Arctic cloud amounts in the CCSM3 climate model. *J. Climate,* **21,** 5673–5687.

——, M. Holland, and D. Bailey, 2011: Changes in Arctic clouds during intervals of rapid sea ice loss. *Climate Dyn.,* **36** (7–8), 1475–1489, doi:10.1007/s00382-010-0816-0.

——, D. Bailey, B. Blazey, M. M. Holland, A. Jahn, and J. Maslanik, 2012: Twenty-first-century Arctic climate change in CCSM4. *J. Climate,* in press.

Woodgate, R. A., and K. Aagaard, 2005: Revising the Bering Strait freshwater flux into the Arctic Ocean. *Geophys. Res. Lett.,* **32,** L02602, doi:10.1029/2004GL021747.

Zhang, X., and J. E. Walsh, 2006: Toward a seasonally ice-covered Arctic Ocean: Scenarios from the IPCC AR4 model simulations. *J. Climate,* **19,** 1730–1747.